OBSERVED DECADAL VARIATIONS OF THE ZONAL MEAN HYGROPAUSE AND ITS RELATIONSHIP TO CHANGES IN THE TRANSPORT BARRIER

A Dissertation
Presented to
The Academic Faculty

by

Marilee May Roell

In Partial Fulfillment
of the Requirements for the Degree
Doctor of Philosophy in the
School of Earth and Atmospheric Sciences

Georgia Institute of Technology
December 2012

OBSERVED DECADAL VARIATIONS OF THE ZONAL MEAN HYGROPAUSE AND ITS RELATIONSHIP TO CHANGES IN THE TRANSPORT BARRIER

Approved by:

Professor Rong Fu, Advisor
School of Earth & Atmospheric Sciences
Georgia Institute of Technology
Jackson School of Geosciences
University of Texas at Austin

Professor Peter Webster
School of Earth & Atmospheric Sciences
Georgia Institute of Technology

Professor Robert Black
School of Earth & Atmospheric Sciences
Georgia Institute of Technology

Dr. Bruce Doddridge
Chemistry and Dynamics Branch, Science Directorate
NASA Langley Research Center

Professor Irina Sokolik
School of Earth & Atmospheric Sciences
Georgia Institute of Technology

Date Approved: 16 August 2012

To my parents,

Marilyn Sopina and Timothy Roell,

who succeeded in laying a good foundation

for all that I have accomplished.

ACKNOWLEDGEMENTS

First, I must acknowledge the contributions made on my outlook on life by those who made it possible for Bugs Bunny to prevent Marvin the Martian from blowing up Earth because it obscured his view of Venus. The absurdly quirky lessons so intelligently and humorously presented have allowed for many hours of entertainment and situational humor during times of stress and conflict. As The Doctor would say, "It was brilliant".

I wish to acknowledge the guidance and encouragement I received from my advisor Dr. Rong Fu, who made this work possible. I am also grateful for the gift of Dr. Jonathon Wright's time and expertise during the completion of this work.

I wish to thank Dr. Irina Sokolik, Dr. Peter Webster, Dr. Robert Black and Dr. Bruce Doddridge for the sharing of their vast knowledge and for being on my committee. I am also grateful to my colleagues at Langley Research Center who selflessly shared their knowledge and time to provide me with the tools necessary to be successful in this endeavor. Dr. Larry Thomason, Dr. Ellis Remsberg and Ms. Sharon Burton encouraged me from the very beginning and were always available to answer questions and provide guidance during my research.

Dr. Charles Hill has been an invaluable resource of knowledge in all areas of importance from statistical and data analysis to how to use various software applications. His encouragement and humor has provided for a fulfilling and satisfying completion of this work and I look forward to many more hours of discussion over such topics as: "Why string theory is wrong"; "The benefits of LaTeX over Microsoft Word"; and "Which Doctor is the best Doctor Who".

I wish to express my gratitude to the NASA Graduate Studies Program which funded this research. Of the many people responsible for encouraging and supporting me during this program of study, Mr. George Allison and Dr. Lelia Vann most deserve my thanks for allowing me to participate and complete this work.

I wish to acknowledge the support of my colleagues and the staff at the school of Earth and Atmospheric Sciences who made it possible for me to do my research away from the school. Dr. Katia Fernandes, Ms. Angelica Remolina, and Ms. Kathy Plummer provided invaluable support during the many trips between school and work by allowing access to computer facilities, software code, and paperwork submittals that relieved much of the stress of doing my research away from GaTech.

I would like to thank my many teachers who encourage me to explore and add to my understanding of the universe. Ms. Weeks, Dr. Barber, and Mr. Hess allowed me to see the wonders of this universe while at the same time instilling knowledge and values that formed the foundation for much of my studies into my adult life. Special thanks goes to Dr. John Reagan who put a high school graduate to work recording solar radiometer data resulting in employment at Langley Research Center where I have a ring side seat to all the wonders of space exploration and planetary research.

Finally, the love and encouragement that my friends and family have provided made this journey much easier. They never lost their sense of humor and remind me about the absurdly quirky nature of the Universe thereby allowing me see the Earth as something other than an obstacle obscuring my view of Venus.

TABLE OF CONTENTS

LIST OF FIGURES

LIST OF SYMBOLS OR ABBREVIATIONS

ATMOS	Atmospheric Trace Molecule Spectroscopy.
B-D	Brewer-Dobson.
DJF	December, January, February.
DJFM	December, January, February, March.
ECMWF	European Centre for Medium-Range Weather Forecasts.
EOS	Earth Observing System.
EPV	Ertel's Potential Vorticity.
ERA-40	ECMWF 40 Year Re-Analysis.
ERBE	Earth Radiation Budget Experiment.
GEOS-5	Goddard Earth Observing System Model, Version 5.
GMAO	Global Modeling and Assimilation Office.
HALOE	HALogen Occultation Experiment.
JJA	June, July, August.
LEO	Low Earth Orbit.
LIMS	Limb Infrared Monitor of the Stratosphere.
LS	Lower Stratosphere.
MAM	March, April, May.
MERRA	Modern Era Retrospective-analysis for Research and Applications.
MLS	Microwave Limb Sounder.
NASA	National Aeronautics and Space Administration.
NCAR	National Center for Atmospheric Research.
NCEP	National Centers for Environmental Prediction.
NH	Northern Hemisphere.
ppmv	parts per million by volume.
ppv	parts per volume.

PV	Potential Vorticity.
PVU	Potential Vorticity Unit.
QBO	Quasi-Biennial Oscillation.
SAGE II	Stratospheric Aerosol and Gas Experiment II.
SH	Southern Hemisphere.
SON	September, October, November.
SST	Sea Surface Temperature.
TTL	Tropical Tropopause Layer.
UARS	Upper Atmosphere Research Satellite.
UT	Upper Troposphere.
V5	Version 5.
V6	Version 6.

SUMMARY

Long term variations in the lower stratospheric water vapor can have a significant influence on the radiative balance and ozone chemistry of the lower stratosphere. Satellite data allowing a global view of the stratospheric water vapor have only been available since the late 1970s providing a nearly continuous 30-year record of stratospheric water vapor. This study examines the long term record of lower stratospheric water vapor focusing on the 20-year data record from the Stratospheric Aerosol and Gas Experiment II (SAGE II). Comparisons between SAGE II lower stratospheric water vapor and the results from other data products are also examined. This study further focuses on the minimum lower stratospheric water vapor (i.e., hygropause) and on the dehydration seen in the hygropause with examination of the transport barrier at both the tropical tropopause and the tropopause folding region between the tropics and extra-tropics that would account for this decadal variation.

In order to use the SAGE II water vapor product, the effects of aerosol contamination from four volcanic eruptions from 1984 to 1992 were examined, leading to a four level filtering of the SAGE II water vapor data to allow retention of good data from early in the data record. With the improved, filtered water vapor data, monthly and seasonal time series analyses show a significant decadal variation in the lower stratosphere for all months where the satellite coverage provided data from the late 1980s to the early 2000s. This decadal variation documents a decrease in the water vapor from below approximately 25 km to below the tropopause with this decrease seen in the hygropause from the tropics to the poles. Comparisons of SAGE II water vapor data with Limb Infrared Monitor of the Stratosphere (LIMS), Microwave Limb Sounder (MLS), and HALogen Occultation Experiment (HALOE) highlight a

consistent picture of water vapor variations over this decadal time frame which highlighted a change in the water vapor pattern that suggests a rising hygropause in the lower stratospheric column of the deep tropics to a poleward horizontal spreading of the hygropause.

Variations seen in the long-term hygropause drying from the tropics to the poles require examination of three transport mechanisms at the regions around the tropopause for the months/season preceding the seasonal minimum. The water vapor minimum in the lower stratosphere was determined from SAGE II water vapor data. Analysis of the hygropause for all months provided a consistent neutral or decreasing value in the long-term water vapor minimum. March was shown to be the seasonal minimum in the hygropause over this 20-year low aerosol record, followed by a discontinuity in the minimum abundance after 2000.

From the analysis performed on the SAGE II data at all levels of the stratosphere, the long-term decline in water vapor in the lower stratosphere was statistically significant. It was clear that the drier air affecting the lower stratosphere was not entering from the top of the stratosphere, because air is dominated by rising motion in the tropics. The tropical tropopause was examined to determine if there was broadening of the tropical circulation that would account for the characteristics of the tropical hygropause in the sub-tropical and extra-tropical regions of the tropopause for the months of December through April. The relative changes between the heights of the tropopause and the hygropause in the latitude regions away from the tropical minima of approximately 1 km did not produce any statistically significant indication of seasonal long-term poleward broadening of tropical circulations for the season prior to the March minimum.

The tropical tropopause temperatures were examined using the new Modern Era Retrospective-analysis for Research and Applications (MERRA) data set. Analysis showed a significant decrease in the tropical and sub-tropical tropopause temperatures

over the 20-year time frame for the DJF season preceding the March minimum. The lower temperatures would provide a colder "cold trap" at the tropopause, further "freeze drying" the air seasonally transported from the upper troposphere to the lower stratosphere, providing the long-term dehydration in the hygropause and lower stratosphere.

To examine the transport pathway of moist upper tropospheric air into the lower stratosphere at the sub-tropical and extra-tropical latitudes, the Ertel's Potential Vorticity (EPV or PV) was examined as a proxy for the sub-tropical jet movement towards the poles over this long-term record. Changes in this pathway location may affect the efficiency of isentropic transport of moist tropospheric air into the lower stratosphere at these higher latitudes. Since the sub-tropical jet resides in-between the EPV contour levels of ± 2 PVU and ± 4 PVU, a change in the location of these contour lines would indicate a change in the sub-tropical jet location. Analysis using the MERRA zonal EPV and maximum zonal Uwind data showed a significant shift in the locations of the contours towards the poles over this 20-year time frame for the DJF, DJFM seasons and the month of December. Whereas this does indicate a shift in the sub-tropical jet location as bounded by the EPV contours of -2 PVU and -4 PVU, the zonal gradient in EPV between these contours and the zonal maximum Uwind did not indicate that the strength of the extra-tropical transport barrier had statistically changed. This study concludes with a discussion of how the transport barrier in the tropics and subtropics, where colder tropopause temperatures have been shown to occur along with the increasing Brewer-Dobson circulation just above the tropopause, are the likely cause for the decreasing water vapor trend as seen in the SAGE II March hygropause over the 20 years from 1986–2005.

CHAPTER I

INTRODUCTION

Water vapor is generally considered the dominant greenhouse gas in the atmosphere because of its abundance in the atmosphere and its radiative properties (Sokolik, 2008). Water vapor absorbs infrared radiation over a wide spectral band continuum and is a source of the ozone destroying hydroxyl radical, introducing competing effects on the temperature of the stratosphere (Forster and Shine, 1999). Although climate science research focuses on the longer lasting greenhouse gases, such as carbon dioxide and methane, and their feedback mechanisms (Solomon et al., 2007, IPCC Technical Report), there is still uncertainty as to the magnitude of the effects of water vapor and its feedback mechanisms in the lower stratosphere on the long term temperature and circulation of the lower stratosphere (Forster and Shine, 2002). Some of the uncertainty for predicting long term climate variation in the lower stratosphere and Tropical Tropopause Layer (TTL) stems from a lack of knowledge as to the global long term trend in water vapor in this region of the atmosphere and the mechanisms that can affect the long term water vapor availability in the lower stratosphere.

Observations from balloon-borne measurements from the 1980s to 2000 provided some evidence that lower stratospheric water vapor was increasing, causing a cooling effect in the stratosphere but inversely warming the troposphere (Dvortsov and Solomon, 2001; Rosenlof et al., 2001; Oltmans et al., 2000). Since 2000, observations have shown that lower stratospheric water vapor decreased, possibly warming the lower stratosphere, while cooling the tropospheric temperatures (Solomon et al., 2010; Randel et al., 2006). Other studies show that while the water vapor is decreasing in the lower stratosphere, the temperature is also decreasing in the same region,

possibly because of the loss of aerosols from volcanic eruptions in the 1980s and 1990s (Thompson and Solomon, 2009). Lack of a good, continuous, long term global record of the vertical profile of water vapor in the lower stratosphere, along with a lack of observations that completely describe how water vapor enters the lower stratosphere, have contributed to some uncertainty as to the water vapor trends globally, the mechanisms that produce those trends, and therefore the effects on the overall global climate from lower stratospheric water vapor.

The long term water vapor variations in the lower stratosphere and the mechanisms behind those decadal variations have been of interest in climate science for decades. How and where the air is dehydrated as it moves from the moist upper troposphere into the lower stratosphere has been studied using various observational and modeling data from balloon borne hygrometers, to satellite sensors, to *in-situ* aircraft flights with observations compared to model results. All observations and models point to the transport barrier at the tropopause and the circulation patterns just above and below the tropical tropopause as mechanisms that affect the total lower stratospheric water vapor (Fueglistaler et al., 2009).

Figure 1.1 shows a schematic of the transport and zonal mean circulations associated with movement of air from the upper troposphere into the lower stratosphere taken directly from Fueglistaler et al. (2009). Of interest to this study, the schematic highlights five areas of transport across the transport barrier of the tropopause, including (a) the small amount of rapid convective moisture that might pass through the tropical tropopause (the moisture could be transported isentropically along the 360 K potential temperature contour into the mid-latitude lower stratosphere), (b) the subsidence feature in the sub-tropics and (c) the sub-tropical jet, which limits transport across the tropical-to-extra-tropical barrier, and (e) the rapid meridional transport, sometimes designated "the lower Brewer-Dobson circulation", which would move moist/dehydrated air rapidly to the poles along isentropic contours

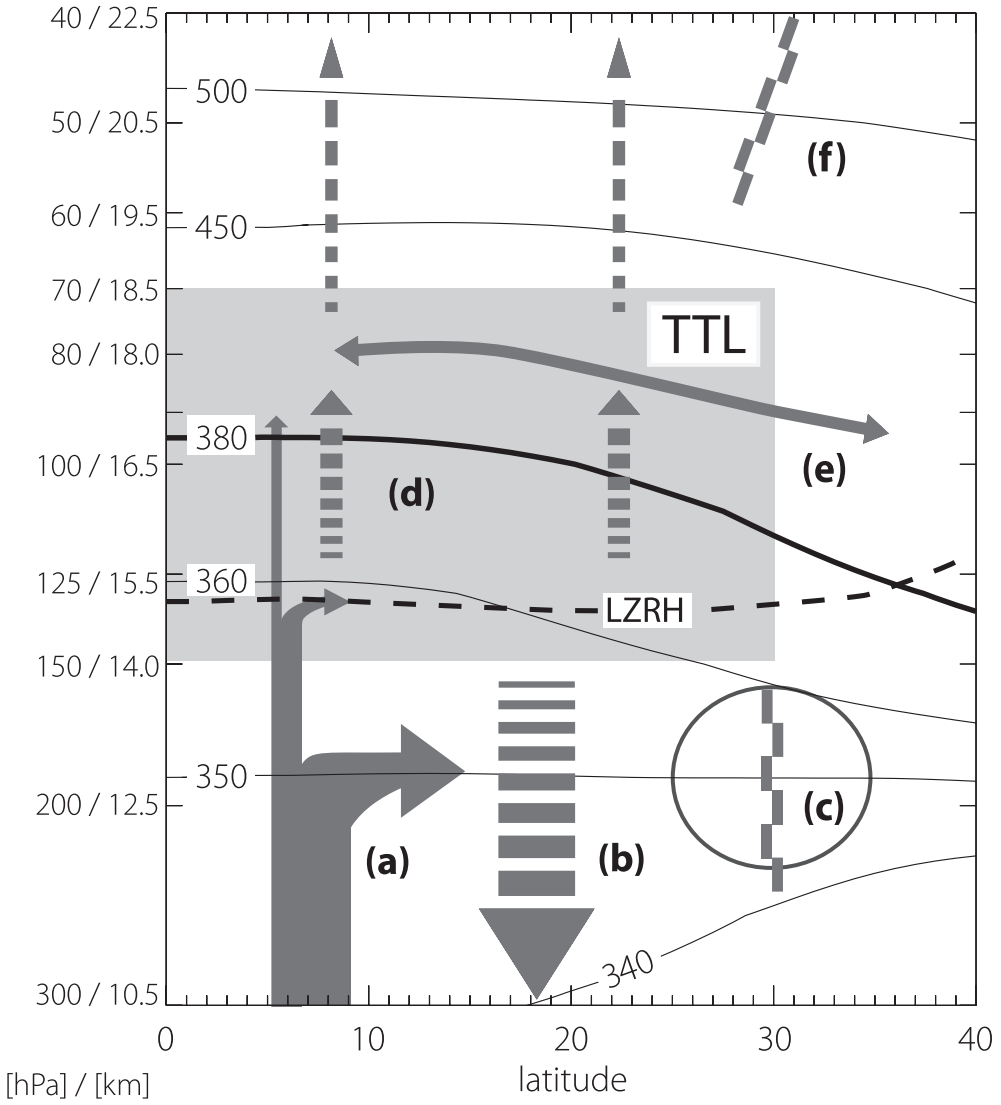

Figure 1.1: Schematic transport and zonal mean circulation taken directly from Fueglistaler et al. (2009) showing (a) the three zonally averaged levels of convective outflow, (b) radiative cooling, (c) the sub-tropical jet, (d) radiative heating, (e) rapid meridional transport above the tropopause, and (f) the tropical pipe.

just above the tropopause. Conversely, the radiative effects of the lower stratospheric water vapor on the tropospheric circulation can feed back on the transport of water vapor through the transport barriers (Tandon et al., 2011) causing circulation changes that further enhance or reduce water vapor transport across the tropopause.

Deep convective transport of water vapor across the tropical tropopause—letter (a) in Figure 1.1—was first postulated by Brewer (1949) and defined as part of the circulation where air moves through the tropopause into the upper stratosphere, then moves to the higher latitudes where it radiatively cools and descends to the lower stratosphere and troposphere (Dobson, 1956). The Brewer-Dobson circulation provided a means for moist tropopause air to move through the tropical tropopause "cold trap", dehydrating the air mass to levels between 2–6 ppmv (Oltmans and Hofmann, 1995; Hintsa et al., 1998) depending on the tropopause temperature. Tropopause temperatures are seasonal, and observations have shown that cold tropopause temperatures produce seasonally drier lower stratospheric air above the tropical tropopause. If the upper Brewer-Dobson circulation were the only pathway for water vapor to move into the mid- and high latitudes, then the lower stratospheric water vapor would have the mixing ratios of the upper stratospheric descending air. Methane oxidation provides upper stratospheric water vapor mixing ratios in the mid- and high latitudes that do not match those found in the lower stratosphere in the same latitudes (Dessler and Sherwood, 2004). Therefore, other pathways exist for transporting air into the lower stratosphere in the mid- and high latitudes. One recent postulation is for the existence of a lower branch of the Brewer-Dobson (B-D) circulation that rapidly moves air in the lower stratosphere from just above the tropical tropopause to the mid- and high latitude lower stratosphere along isentropic surfaces (Ray et al., 2010) as represented by (e) in Figure 1.1. This is an extension of the isentropic transport mechanism proposed by Hoskins (1991), Holton et al. (1995), and Dessler et al. (1995) for moving

air across the mid- and high latitude tropopause along the isentropic surfaces below 380 K.

Evidence for isentropic transport from the Upper Troposphere (UT) to the Lower Stratosphere (LS) at the mid-latitudes was provided by Poulida et al. (1996), Rood et al. (1997), Hintsa et al. (1998), Ray et al. (2004), and Dessler and Sherwood (2004) from observational data showing insertion of UT air across the sub- and extratropical tropopause into the LS through the process of deep convective transport. Wang (2003) performed modeling work that provided a mechanism for water vapor transport from the top of deep convective anvil clouds diabatically into the LS, where it then moved adiabatically along isentropic surfaces in the stratosphere. Schoeberl (2004) added support to the isentropic surface cross-tropopause pathways through the estimation of the air mass flux from the downward diabatic cross-tropopause exchange between the lower stratosphere and the upper troposphere, which was five times that available from the B-D circulation downward exchange of air mass from the upper stratosphere to the lower stratosphere. Another pathway for transport of tropospheric air masses across the transport barrier occurs at the sub-tropical jet location. A strong sub-tropical jet, characterized by strong PV gradients, tends to cut-off isentropic transport across the tropopause (Holton et al., 1995). Estimations of how much water vapor is irreversibly transported isentropically into the lower stratosphere have not been determined because of the complexity of potentially competing pathways and the difficulty in finding a realtime proxy to track this pathway across the transport barrier. Recent studies have investigated how the isentropic transport can be reduced or enhanced through upper atmospheric circulation changes in the sub-tropics and mid-latitudes (Haynes and Shuckburgh, 2000).

The seasonal sub-tropical jet—letter (c) in Figure 1.1—is located at the poleward edge of the Hadley circulation. The seasonal strength and location of the Hadley circulation can affect the location of the subsidence of air masses in the tropical/subtropical

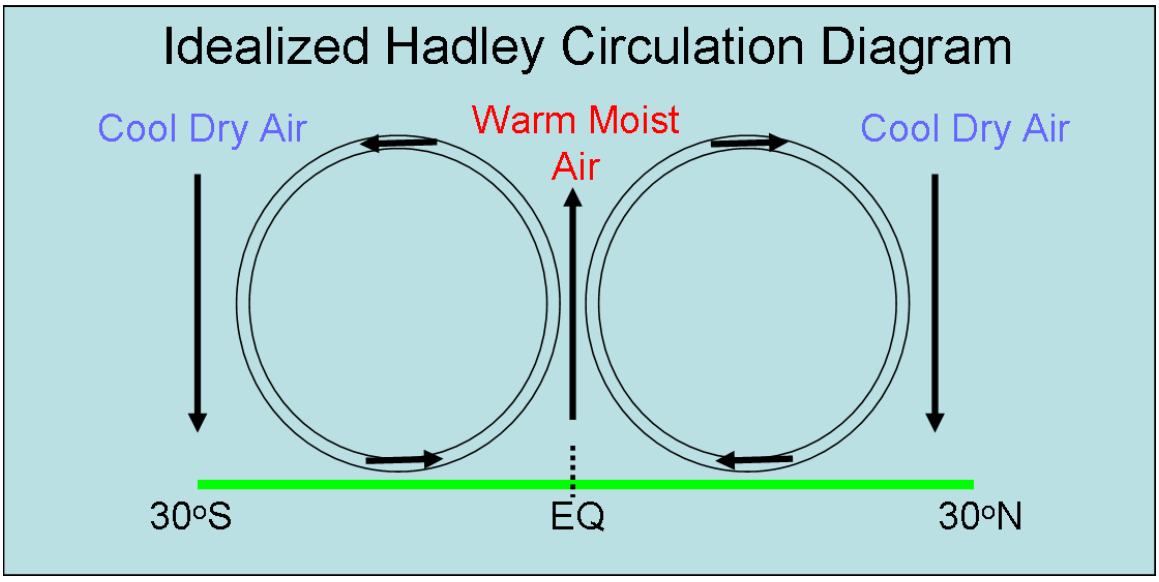

Figure 1.2: Schematic of Hadley circulations in the troposphere.

latitudes—letter (b) in Figure 1.1. Changes in the location of the descending edge of the Hadley circulation therefore affect the terrestrial location for rainfall in the subtropical latitudes affecting millions of people on the planet (Webster, 2004). Figure 1.2 shows an idealized schematic of the Hadley circulation for both hemispheres showing the locations of the ascending and descending air masses. Recent findings have shown that the sub-tropical jet has moved poleward over the last 30 years (Seidel et al., 2007; Hudson, 2011) with concurrent indications of a broadening of the seasonal Hadley cell towards the poles (Hu and Fu, 2007). There are also indications that the sub-tropical jets have weakened and moved higher in altitude (Archer and Caldeira, 2008).

This thesis will present the decadal pattern of variations in the monthly averaged lower stratospheric water vapor and water vapor minimum (or hygropause as defined by Kley et al., 1979) for the Southern Hemisphere preceding the annual water vapor minimum over the 20-year SAGE II data record from 1986–2005. Chapter 2 introduces the data and methodology for this study; Chapter 3 details the decadal variations in the lower stratospheric water vapor and hygropause; Chapter 4 examines

the mechanisms for the observed changes at the transport barrier along the tropical, sub-tropical and extratropical tropopause that can explain the observed decadal variations in the lower stratospheric water vapor; and Chapter 5 provides a discussion of the mechanisms studied and planned future work in this area.

CHAPTER II

DATA AND METHOD

2.1 Data

Over the last three decades, satellite instruments have observed stratospheric water vapor with varying degrees of temporal and spatial coverage and varying measurement precision and accuracy. The difficulty in discovering decadal climate variations in the stratospheric water vapor is in recovering a long-term record of observed water vapor from the few satellite data sets available up to 2005. This is made even more difficult when column measurements are used requiring the removal of tropospheric water vapor from the measurement to infer stratospheric water vapor values. To avoid the large uncertainty that column measurements introduce into the lower stratospheric water vapor retrievals, satellite instruments that measured water vapor vertical profiles are used to highlight the 30 year record of lower stratospheric water vapor features. This study undertakes the analysis of three satellite data sets that observe the water vapor vertical profiles from ∼3 hPa to ∼100 hPa to show changes in the stratospheric water vapor from 1979 to 2005.

2.1.1 SAGE II

The Stratospheric Aerosol and Gas Experiment II (SAGE II) instrument was aboard the Earth Radiation Budget Experiment (ERBE) satellite, which was deployed from the Space Shuttle Challenger on October 5, 1984 into a nominal 56° inclination, 610 km circular orbit. The SAGE II instrument employed a seven-channel sunphotometer to measure aerosols (four channels at 1.02 μm, 0.525 μm, 0.453 μm, and 0.385 μm), ozone (0.6 μm), water vapor (0.94 μm), and nitrogen dioxide (0.448 μm and 0.453 μm using differential absorption) at each sunrise and sunset using the solar

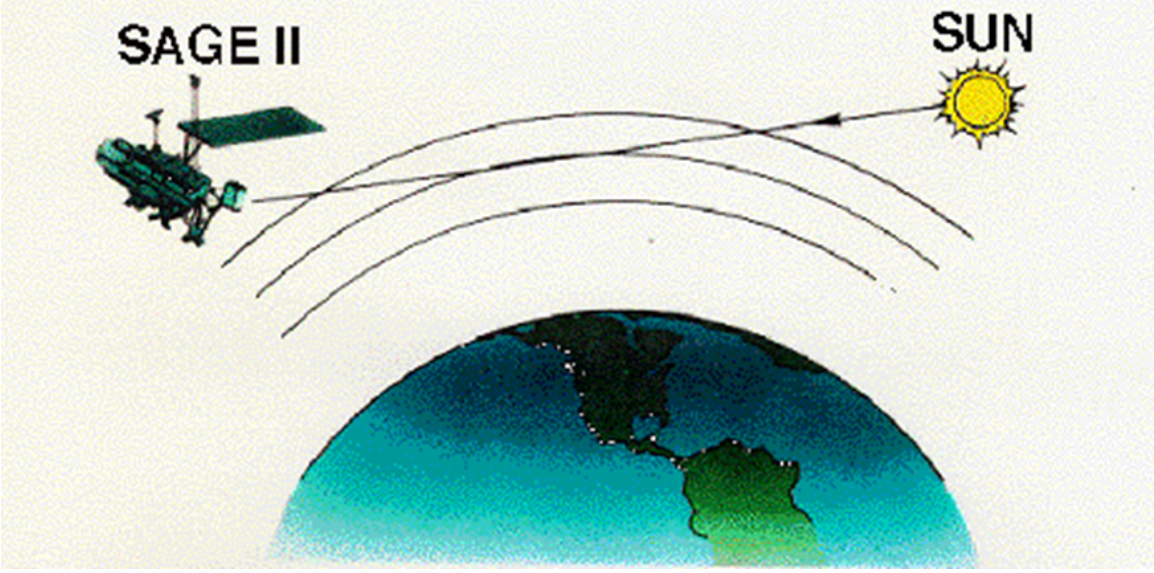

Figure 2.1: Schematic of the solar occultation technique that the SAGE II sunphotometer detector employed from an orbit of 610 km. Picture taken from NASA Langley Research Center, Office of Public Affairs (1996), http://www.nasa.gov/centers/langley/news/factsheets/SAGE.html.

occultation technique (Figure 2.1) with an instrument field of view in the directions normal to the Sun's ray of 0.5 km vertically by 5 km horizontally (Cunnold et al., 1989; Yue et al., 1989).

SAGE II provided fifteen sunrise and sunset measurements daily (individually called an "event") distributed evenly in longitude along a latitude circle up to 2000. After 2000, the instrument was operated at 50% duty cycle to conserve the azimuth gimbal system and extend the mission life until satellite shutdown in August 2005 (Taha et al., 2004). Because of the temporal and spatial sparseness of the Low Earth Orbit (LEO) solar occultation sampling, the SAGE II data set does not have daily coverage of the globe, especially in the tropics. Therefore SAGE II data are best used for monthly and seasonal analyses of the atmosphere from $\sim$10 km to 50 km. The monthly mean calculation provides that at any given latitude segment, there are enough events to produce a significant water vapor mean for that latitude bin. Figure 2.2 shows plots of events that make up the 10-degree zonal monthly mean

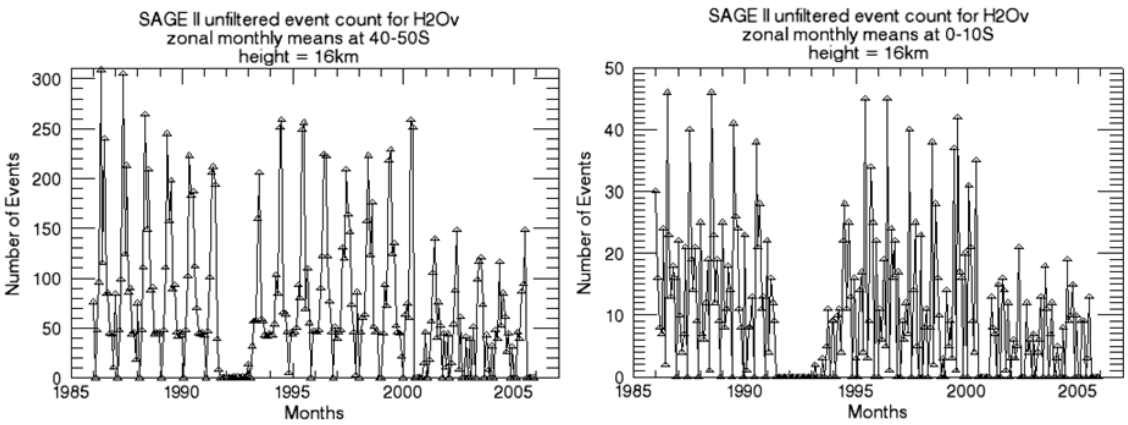

Figure 2.2: Event counts, before quality screening, for two SAGE II zonal (10 degrees in latitude) monthly means from January 1986 to August 2005. Left plot is for Southern Hemisphere mid-latitude; Right plot is for Southern Hemisphere tropical region.

at an altitude of 16 km for the lifetime of the SAGE II instrument for mid-latitude and tropical zonal bins. The tropical latitudes were not well covered by the SAGE II instrument, however the mid–high-latitude event counts for the monthly mean calculation are more significant for eleven months of the year up to the year 2000, when the SAGE II instrument was transitioned to a reduced duty cycle until it was decommissioned in 2005.

The lack of water vapor monthly mean data at 16 km for June 1991 to February 1993, seen in Figure 2.2, reflects the degradation of the water vapor signal caused by the high aerosol influence from the Mt. Pinatubo eruption in June 1991. This volcanic eruption produced approximately 20–30 megatons of aerosol in the lower and middle stratosphere up to 30 km initially in the Northern Hemisphere between 10°S–30°N, with eventual aerosol dispersal into the mid and high latitude lower stratosphere of both hemispheres through dynamic processes of winter stratospheric jet-stream airmass movement (McCormick and Veiga, 1992). Figure 2.3 shows the zonal-mean distribution of aerosol in 20-degree latitude bins in the tropics and midlatitudes over the 20-year SAGE II instrument operation using the SAGE II aerosol product from the

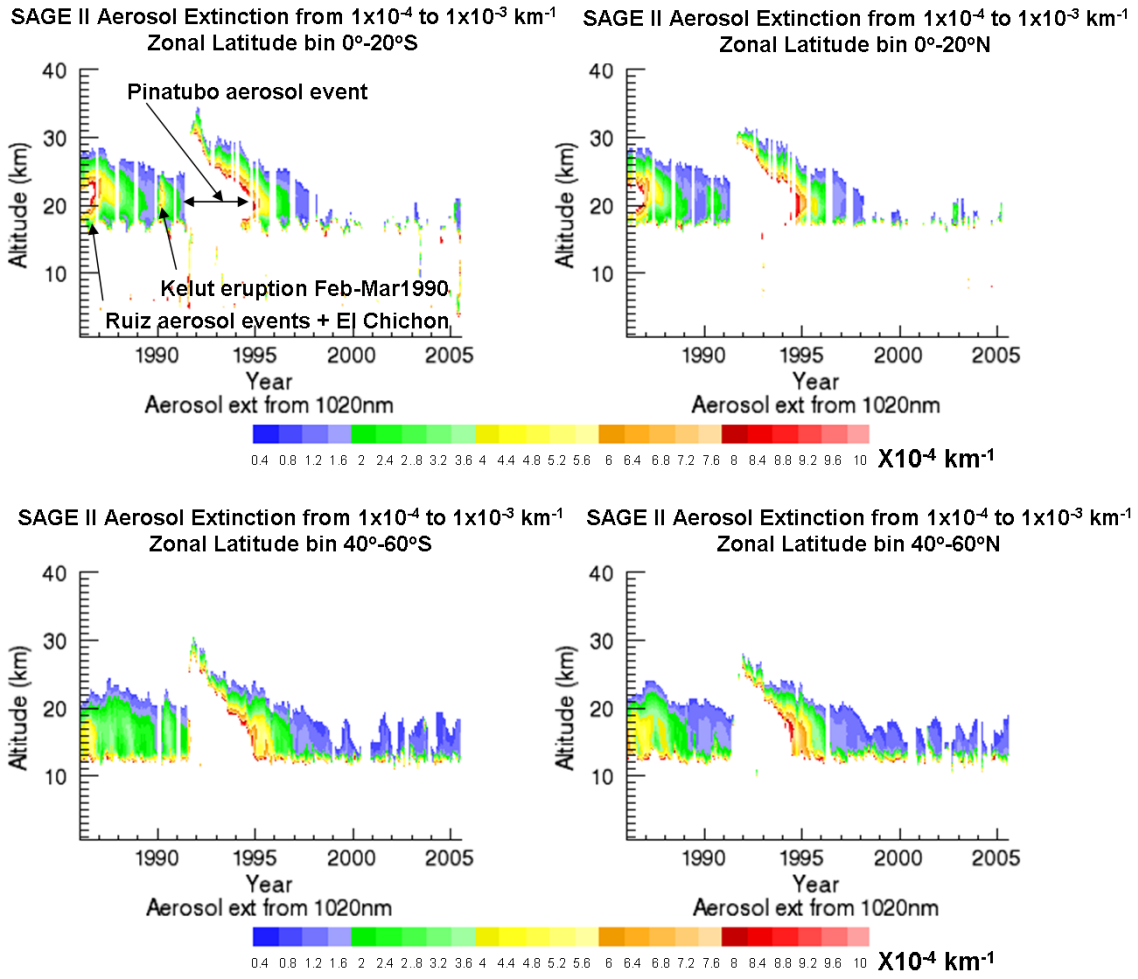

Figure 2.3: Aerosol distribution from 1986 to 2005 using the SAGE II 1020 nm aerosol product. The top two plots show the 20-degree zonal region on either side of the equator, while the bottom plots show the zonal mid-latitude regions of the Earth. Aerosol extinctions from 10^{-3} km^{-1} (red) to 0.4×10^{-4} km^{-1} (blue) are shown.

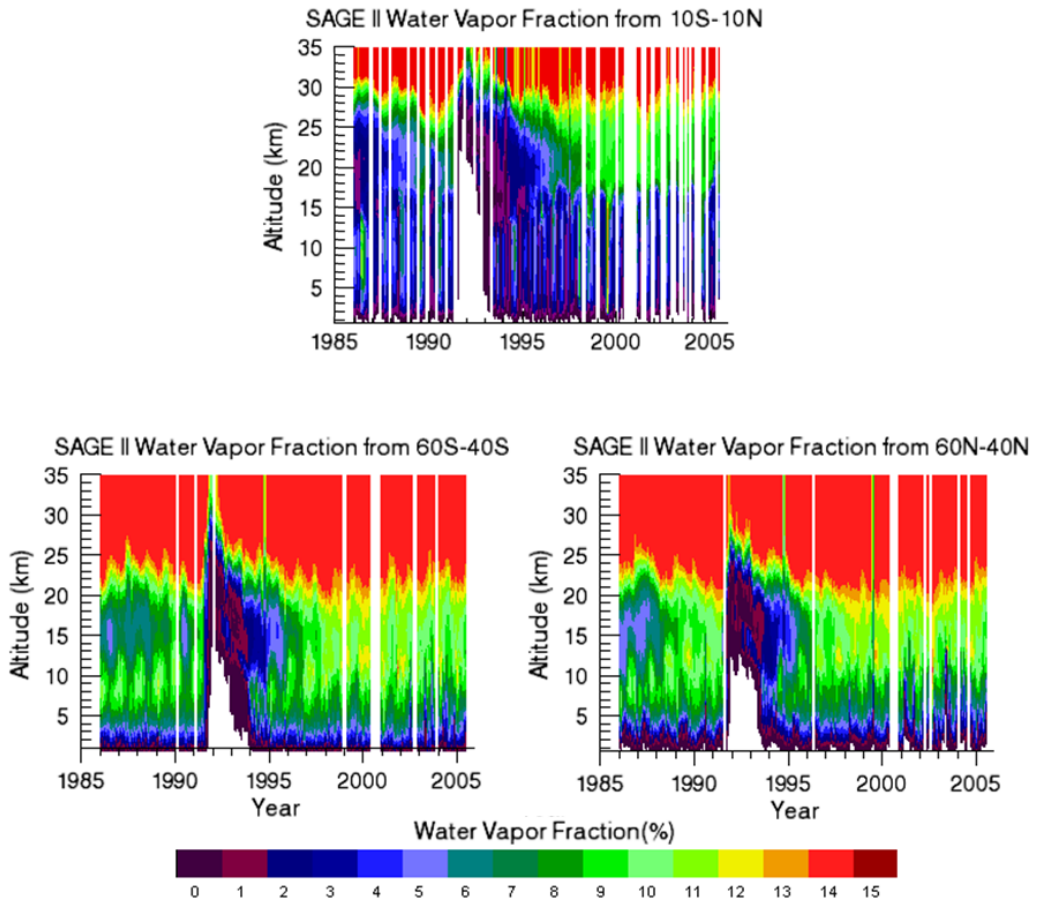

Figure 2.4: Zonal monthly mean water vapor fractions for the SAGE II 940 nm channel. Small water vapor fractions (dark blue to purple) have a higher uncertainty associated with the water vapor mixing ratio measurement.

1020 nm channel. This aerosol product shows the presence of aerosol at various particle densities from multiple volcanic eruptions primarily affecting the stratospheric aerosol layer. Large aerosol extinctions can be seen in the tropics between 18 km and 26 km, and as high as 35 km from Mt. Pinatubo. Relatively large aerosol densities at mid-latitudes are also seen from 12 km to 20 km, with aerosols produced from Mt. Pinatubo up to 30 km. The aerosol extinction ranges up to 10×10^{-4} km^{-1}, with Mt. Pinatubo gases producing the largest amount of aerosol extinctions over a large latitude range of the globe during the 20-year SAGE II data record.

The aerosol influence from the Mt. Pinatubo eruption can clearly be seen in the SAGE II water vapor data (Figure 2.2) as an omission of water vapor signal motivated

by channel saturation, however the effects of that eruption and other aerosol producing events can be seen in the SAGE II data in the mid and tropical latitude plots of the water vapor fraction (Figure 2.4), which is a measure of the fraction of the water vapor absorption contained in the total optical depth signal for the 0.96 μm water vapor channel (Thomason et al., 2004). At water vapor fractions of less than 5%, the uncertainty in the water vapor mixing ratio can increase to greater than 40%, with values of uncertainty as high as 300% were seen following the Mt. Pinatubo eruption at some altitudes and locations resulting from the errors introduced into the water vapor algorithm from the aerosol model.

In October 2003, version 6.2 of the SAGE II water vapor data was released, providing better aerosol modeling that rectified some low-aerosol loading discrepancies in the water vapor signal. Version 6.2 also fixed the apparent drift in the water vapor channel, providing a better fit of the SAGE II water vapor product to the HALOE water vapor product (Thomason et al., 2004). Although version 6.2 has better aerosol modeling algorithms, high aerosol can still adversely affect the water vapor retrieval during the periods of large aerosol extinctions from volcanic eruptions, causing large uncertainties in the water vapor signal at water vapor fractions of less than 5%. Because of the large uncertainty in the water vapor mixing ratio that can occur when aerosol is present, and because of the climatological difference with HALOE water vapor, Thomason et al. (2004) recommended that water vapor data for aerosol extinctions greater than 3×10^{-4} km^{-1} be avoided in climatological studies. However, caution should be taken to not eliminate possible valid water vapor data in the lower stratosphere, as high concentrations of aerosols do not necessarily invalidate the water vapor data, but only contribute to a higher uncertainty in the value for most of the 20-year record (L. W. Thomason, personal communication, April 4, 2009). Taha et al. (2004) used the aerosol threshold of 2×10^{-4} km^{-1} and water vapor mixing ratio uncertainties of greater than 50% to eliminate data and perform comparisons with

HALOE water vapor data for three discrete time periods during coincident instrument operations. Results from that study generally agreed with HALOE data to within 5%, however almost all of the 1985–1995 period of lower stratosphere water vapor is eliminated from the study using this conservative aerosol threshold. In an effort to recover as much of the valid water vapor data as possible for the entire 20-year operation of SAGE II, a different approach to data filtering was undertaken for this thesis study.

The aerosol sensitivity inherent in the SAGE II water vapor signal along with known outliers in the data requires that the SAGE II water vapor data be filtered when calculating monthly means. The filtering criteria used are highly dependent on the size of the latitude/longitude bin and the altitude of interest in the water vapor record, as filtering will eliminate events that make up the monthly means, which affects both the significance of the means and the uncertainties in the mean values. The first filtering criterion was performed on each event collected, and eliminated all water vapor mixing ratios in an event greater than 10 ppmv in the region of interest from the tropopause (and hygropause) to the middle stratosphere ($\sim$35 km). This first filtering criterion produces a water vapor event plot (Figure 2.5) that still includes obviously anomalous mixing ratios that are a result of large aerosol uncertainties during the time frames of known volcanic eruptions in both the tropics and mid-latitudes. The abscissa in Figures 2.5–2.8 shows the cumulative number of events as a consequence of the daily event counts varying over the 20-year SAGE II data record for each latitude bin. The second filtering criterion allows for retention of possibly valid data in the early period of the SAGE II product by setting the filter value for aerosol extinction at the less conservative threshold of 6×10^{-4} km^{-1}.

A side-by-side comparison of the events retained for two aerosol filtering criteria, the conservative filtering of water vapor events for aerosol extinction values greater than 2×10^{-4} km^{-1} applied by Taha et al. (2004), and the less conservative aerosol

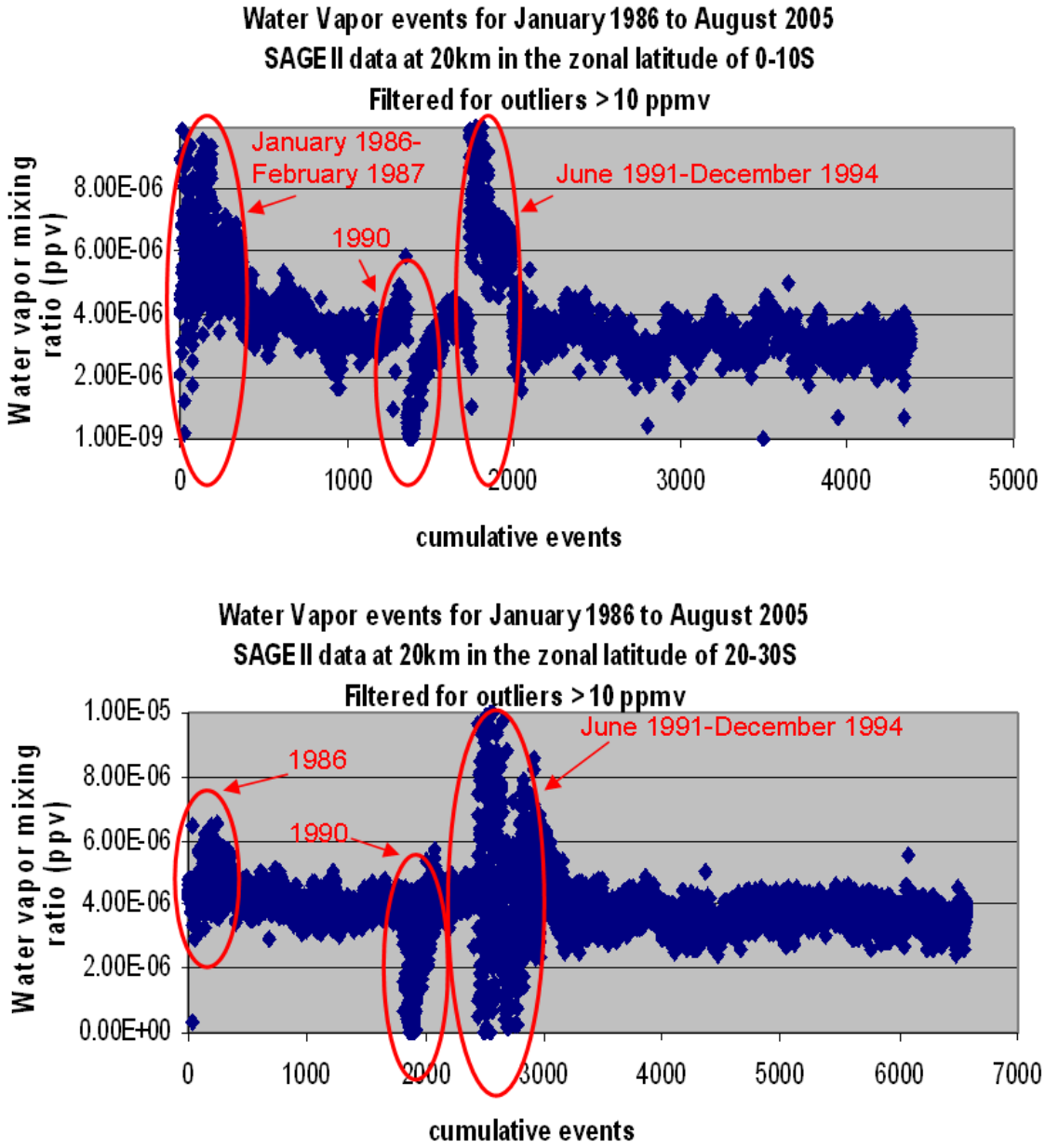

Figure 2.5: SAGE II water vapor mixing ratios for the zonal tropical (top plot) and sub-tropical (bottom plot) regions at 20 km (approximate altitude of maximum aerosol extinction) from January 1986 to August 2005. The x-axis shows the cumulative events recorded (not a time series as daily event counts vary) over that time period. Data have been filtered for outliers greater than 10 ppmv. Dates of events retrieved during periods of volcanic eruptions are highlighted and labeled.

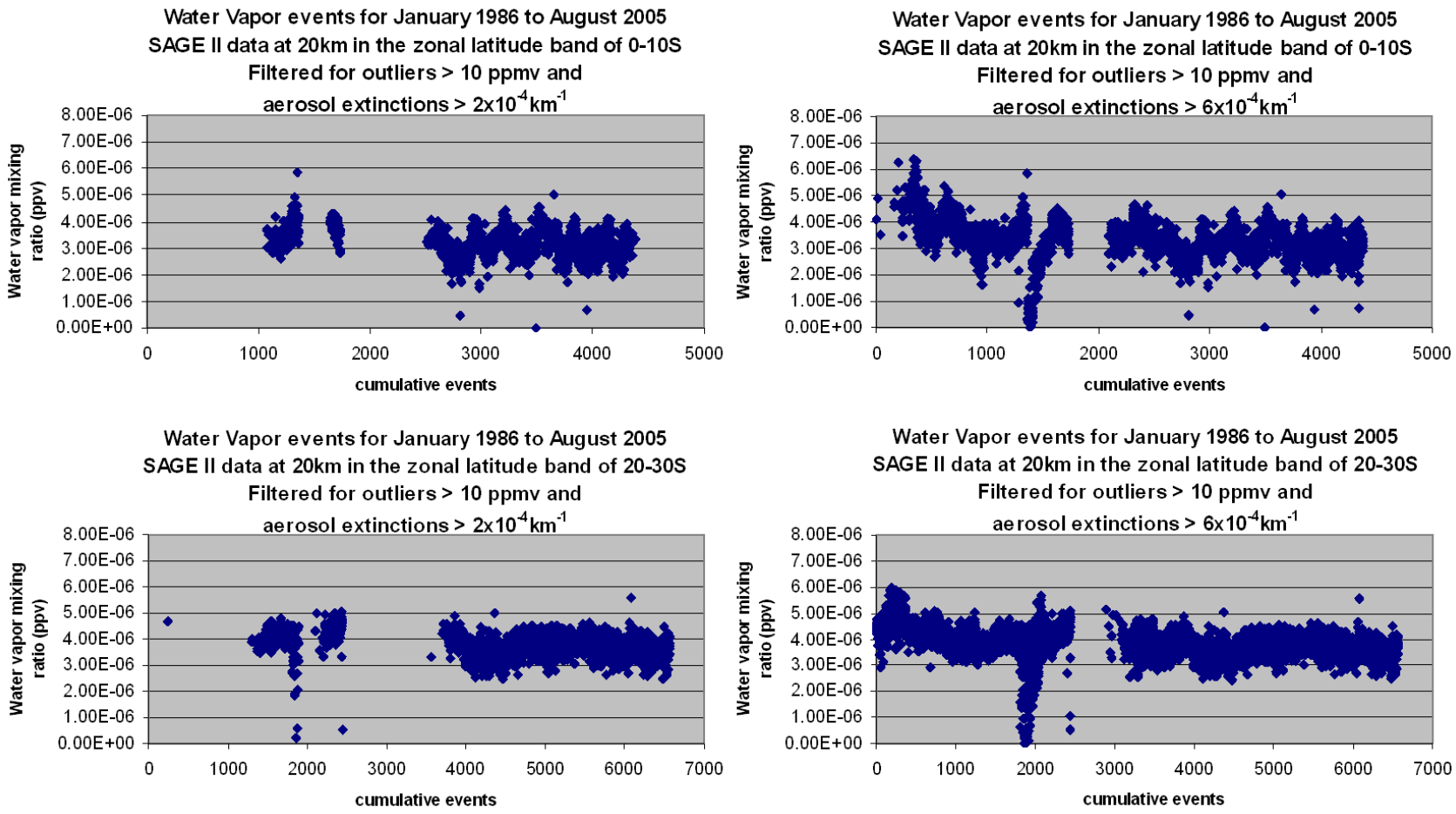

Figure 2.6: SAGE II water vapor events for tropical (top plots) and sub-tropical (bottom plots) zonal regions for the two criteria of the aerosol extinction filtering of 2×10^{-4} km^{-1} (left) and 6×10^{-4} km^{-1} (right) within the 20-year SAGE II record from January 1986 to August 2005. The abscissa is the same as in Figure 2.5.

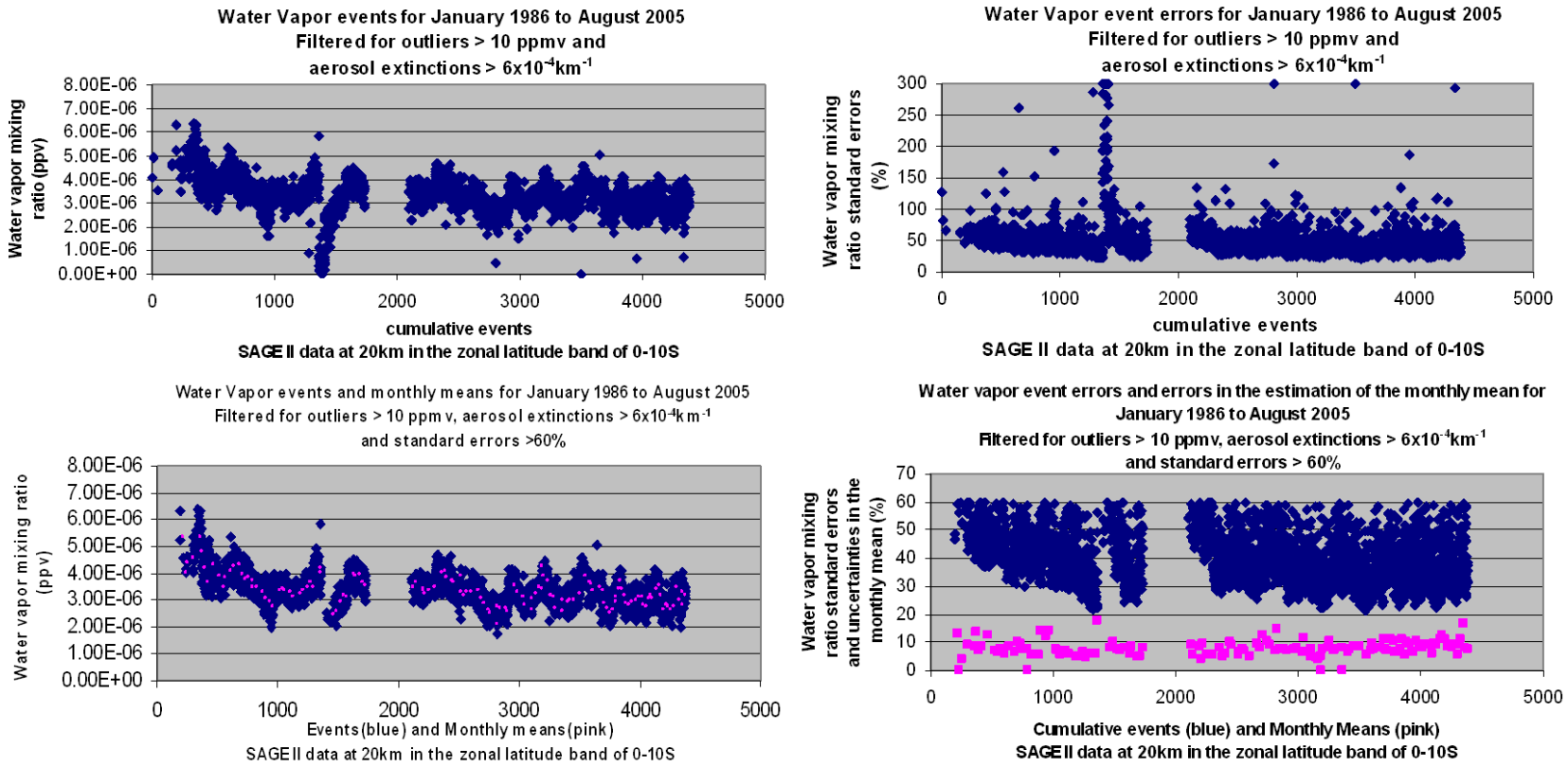

Figure 2.7: Zonal tropical events and event errors at 20 km from January 1986 to August 2005 where the event data were additionally filtered to only include aerosol extinctions less than 6×10^{-4} km^{-1} (top plots) and event standard errors greater than 60% (bottom plots). The monthly means and the errors in the estimations of the monthly means are included on the bottom plots after filtering for the event standard errors greater than 60%. The abscissa is the same as in Figure 2.5.

threshold at greater than 6×10^{-4} km^{-1}, is shown in Figure 2.6. It is apparent that some events in and around 1989 and 1991 are retained even using the conservative aerosol threshold of 2×10^{-4} km^{-1}, however much of the data before 1995 is lost. At first glance, the less conservative approach used by this study retains events that are comparable in mixing ratio with events retained using the aerosol threshold of 2×10^{-4} km^{-1}, supporting the assertion that the early SAGE II water vapor event data, which is eliminated under the method of Taha et al. (2004), might indeed be valid. The standard error on the events for both criteria varies primarily between 20% and 60% with a few ($\sim$10%) exhibiting higher standard errors up to a maximum of about 300%. The highest of these anomalous standard errors occur in the early 1990s and are attributed to the aerosol contamination from the Mt. Kelut volcanic eruption (Figure 2.7).

A third filtering criterion is used to eliminate events with standard errors greater than 60% from inclusion in the calculations of the monthly means. Removing the approximately 10% of events over the 20-year record where the standard errors are greater than 60% does eliminate the early 1990 events retrieved during the Mt. Kelut eruption as well as most of the events in 1986 that exhibit high aerosol contamination as seen in Figure 2.7. The monthly means and uncertainties in the estimations of the monthly means given the events' standard measurement errors, sometimes referred to as the monthly mean uncertainties, are included in the lower two plots, with monthly mean uncertainties mostly at or below 10%. This third filtering criterion improves the mid-latitude data by removing approximately the 3% of events that exceed a 60% standard error limit. Figure 2.8 shows the sub-tropical zonal events and resulting monthly means along with event uncertainties and monthly mean uncertainties from data cleared by the three filtering criteria employed by this study. Once again the monthly mean uncertainties in the estimations of the mean calculated from the events standard errors were mostly at or below 10%, with February 1990 through

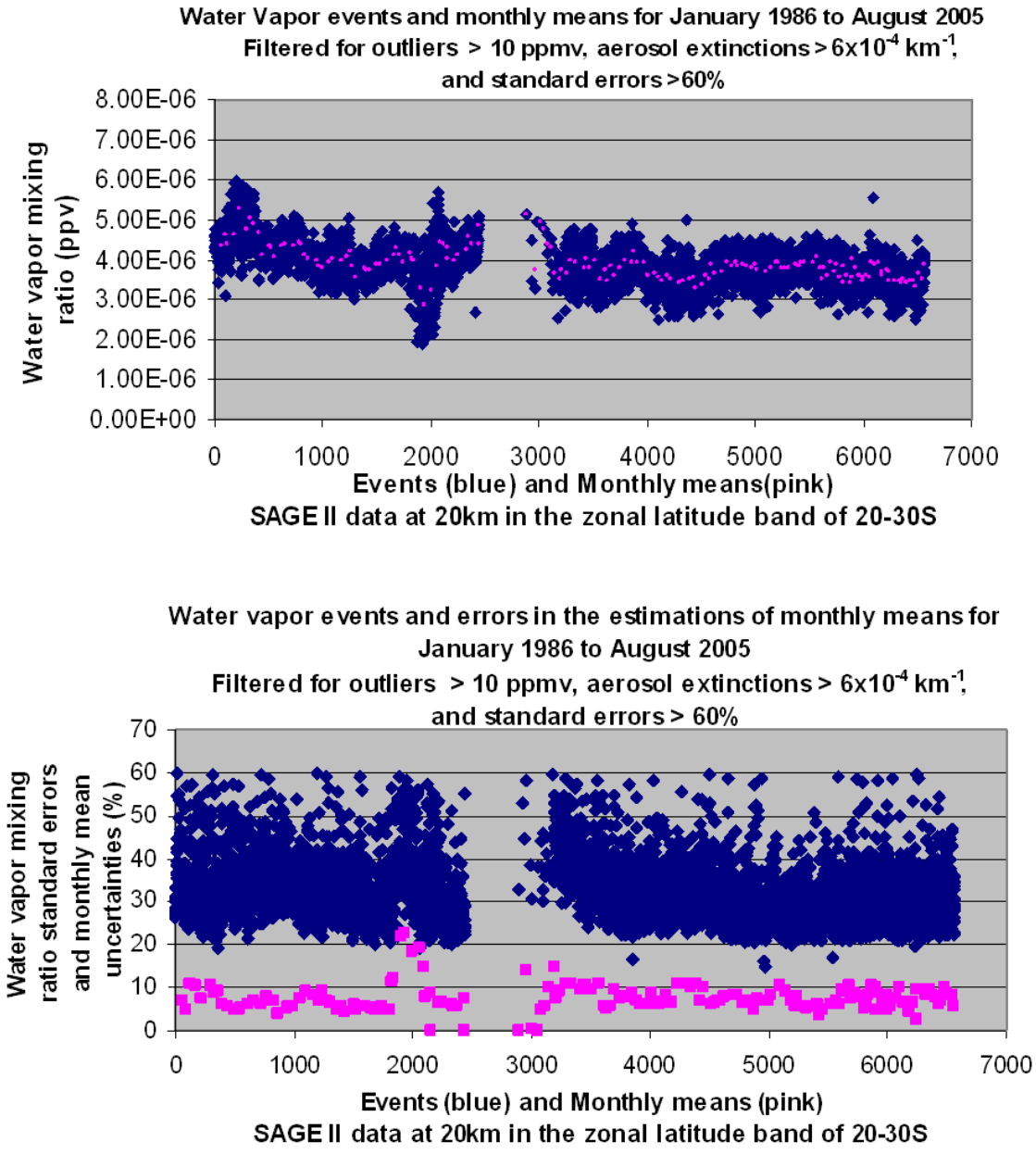

Figure 2.8: The water vapor events and monthly means (top plot) and the event standard errors and errors in the estimations of the monthly means (bottom plot) for the sub-tropical zonal region at 20 km altitude after including all three filtering criteria. The large monthly mean errors at ∼1900 (event count) correspond to the time of the eruption of Mt. Kelut (Feb–Aug 1990).

August 1990 and several months following the eruption of Mt. Pinatubo showing the largest standard errors in the 20-year record. Although the three filtering criteria enforced on the event data so far provides data throughout the 20-year record of SAGE II, additional filtering of the monthly means was used to ensure that the effects associated with the eruption of Mt. Pinatubo and other volcanic activity (e.g., Mt. Kelut and Ruiz) did not affect any long term analysis of lower stratospheric water vapor. Additionally, when only one event was available for calculation of a monthly mean in a given latitude/altitude bin, it was eliminated as a candidate for this analysis.

A comparison of the difference in the monthly mean mixing ratios between the conservative aerosol extinction filtering of 2×10^{-4} km^{-1} and the less conservative aerosol extinction filtering of 6×10^{-4} km^{-1} for two zonal 10-degree bins at three altitudes in the aerosol belt (between 17.5 km and 22 km) is shown in Figure 2.9. Both data sets were filtered for outliers greater than 10 ppmv and for event standard errors greater than 60%. As expected, the largest difference between the two aerosol filtering criteria is seen in the 17.5 km region of the tropical and sub-tropical atmosphere because of the greater likelihood of aerosol contamination in that region just above the tropopause: the months from January 1986 through early 1987 (Mt. Ruiz and El Chichon), February 1990 through August 1990 (Mt. Kelut), and the time of the Mt. Pinatubo aerosol feature (June 1991 through early 1996) show the most difference between the two aerosol filtering methods primarily at the lower altitude of 17.5 km just above the tropopause. The standard error of estimation of the monthly means using the 6×10^{-4} km^{-1} aerosol extinction filter at the three altitudes for the two zonal latitude regions are mostly around the 10% uncertainty range, with the months of the Mt. Kelut and Mt. Pinatubo aerosol contamination as clear outliers of the norm (either zero or much larger than 10% at 22 km) as seen in the sub-tropical latitude bin.

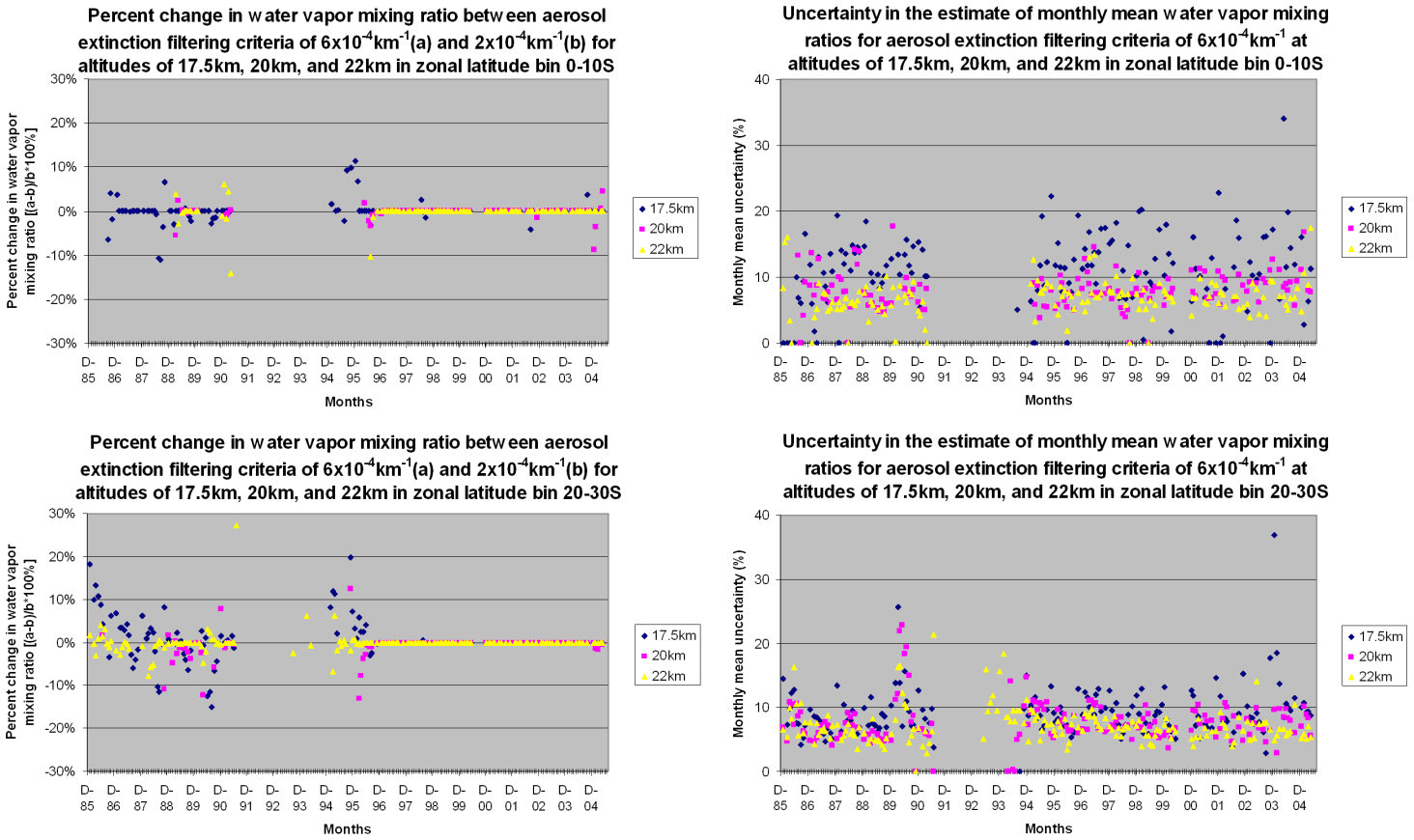

Figure 2.9: Water vapor monthly mean differences between results calculated using the conservative aerosol extinction filtering criteria of $2\times10^{-4}\text{km}^{-1}$ and the less conservative aerosol extinction of $6\times10^{-4}\text{km}^{-1}$ at the three altitudes of 17.5 km, 20 km, and 22 km for the zonal southern tropics and sub-tropical latitude regions (left plots). The right plots show the uncertainties in the estimates of the monthly means for the same altitudes and regions for the less conservative aerosol extinction filtering criteria of 6×10^{-4} km^{-1}.

The difference in the monthly mean water vapor mixing ratio between the two aerosol filtering criteria clearly argue for caution when considering the tropical/sub-tropical lower atmosphere just above the tropopause during the time frame when volcanic eruptions produce aerosols in the stratosphere. Standard errors reported just above the tropopause in the tropics are typically below 20%, decreasing to below 15% in the sub-tropics. For regions higher in the atmosphere (above 20 km), the difference between the two aerosol filtering criteria can be more readily attributed to aerosols especially in the sub-tropics and mid-latitudes (not shown). A quick way to provide better confidence of any long term variations in stratospheric water vapor over the 20-year record is to eliminate the monthly means in 1990 (February–August), and 1991–1994 (June 1991–December 1994), where high aerosol extinctions likely affected the water vapor retrieval significantly in the sub-tropics and mid-latitudes. Also eliminating any monthly means calculated from only one event will improve the confidence in the 20-year monthly mean data record. Some caution should still be exercised when considering the tropical and sub-tropical regions above the tropopause, as that is the region showing the most difference between the conservative and less conservative filtering criteria. These differences, however, are mostly below $\pm 10\%$, which is within the uncertainty range of the HALOE water vapor data set comparison (Thomason et al., 2004). The early part of the SAGE II aerosol record has a decreasing level of aerosol in the mid- and high latitudes compared to the tropics (Figure 2.3). It is because of the smaller aerosol signatures in the extra-tropics that the 1986–1987 monthly means will be retained for use in the analysis of stratospheric water vapor throughout the rest of this thesis with notation where necessary to highlight high standard errors in regions (latitude and altitude) where they occur.

Figure 2.10 shows a comparison of zonally averaged water vapor mixing ratios between data filtered for outliers and the conservative aerosol extinction threshold of 2×10^{-4} km^{-1}, and data filtered for outliers and the less conservative aerosol extinction

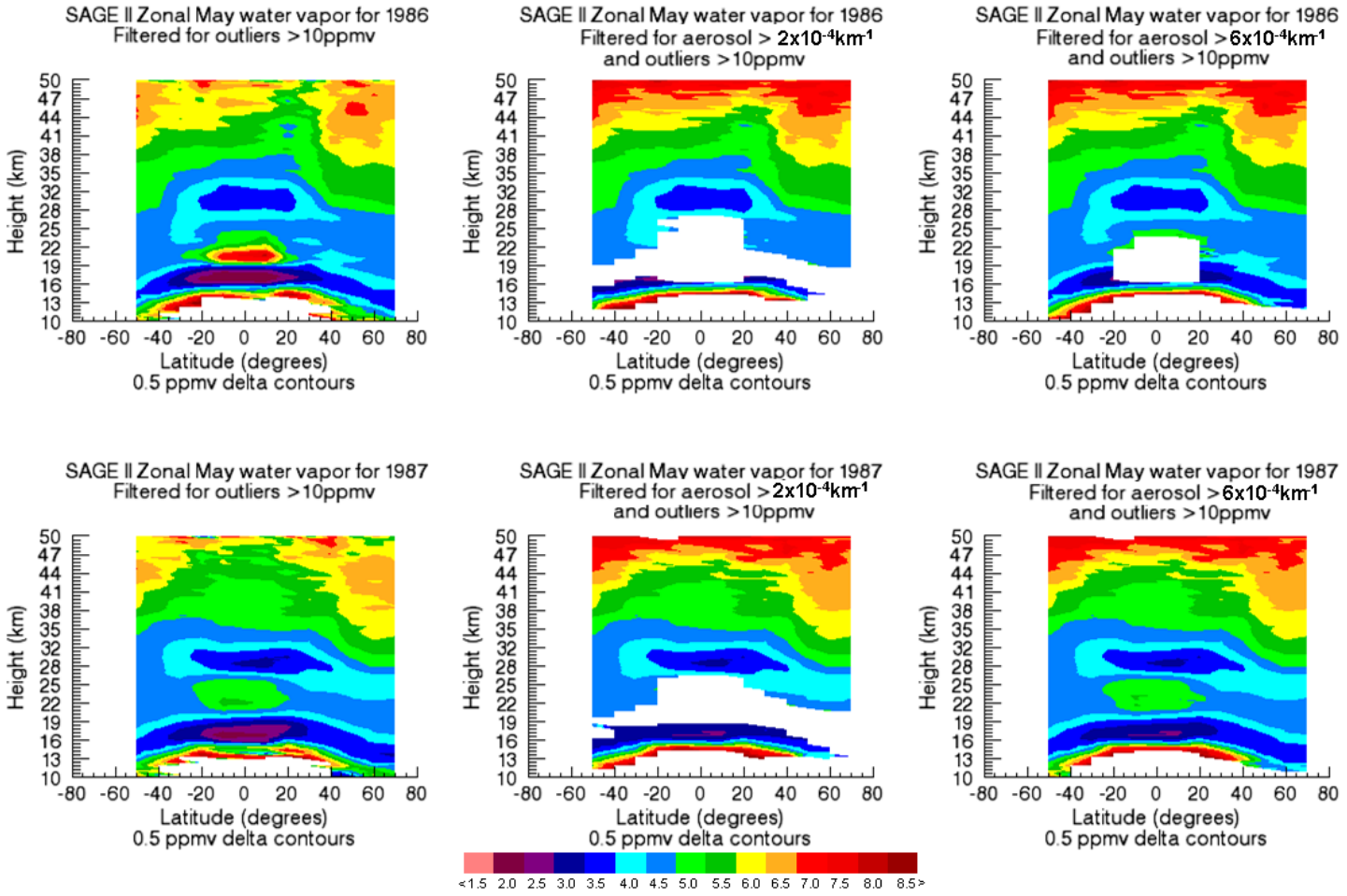

Figure 2.10: Zonally averaged water vapor mixing ratio contour plots for three aerosol extinction filtering criteria (no filtering, conservative filtering, and less conservative filtering) for May 1986 and May 1987. All data are filtered to exclude event standard errors greater than 60%.

threshold of 6×10^{-4} km^{-1} for two May months in the high aerosol years of 1986 and 1987. The disadvantage of filtering the water vapor data using the conservative aerosol threshold of 2×10^{-4} km^{-1} is illustrated in the middle plots of Figure 2.10, where at all latitudes the lower stratospheric water vapor is lost when calculating the monthly means. This effect can be seen in the record for the years from 1986–1989 and 1995–1996 when the high aerosol months in 1990 and 1991–1994 are eliminated. Unfiltered water vapor data (left plots) show the lower stratosphere at all latitudes (10-degree zonal bins), but have anomalously high water vapor mixing ratios over the tropics. The right plots provide visibility of the lower stratosphere at mid- and high-latitudes while filtering for aerosol and outliers and providing an error estimate in the monthly mean of less than 10% in the top of the aerosol band (approximately 20 km–25 km) and less than 20% in the region above the tropical tropopause.

2.1.2 LIMS

The Nimbus 7 Limb Infrared Monitor of the Stratosphere (LIMS) satellite instrument retrieved water vapor profiles (over 7000 profiles per day) from 1978 to 1979 (7.5 months) and provided the first ever near-global product of water vapor measurements of the stratosphere. LIMS used a six channel infrared radiometer (wavelengths centered between 6 μm and 15 μm) to scan the limb of the atmosphere for CO_2 (two bands straddling 15 μm), Ozone (9.6 μm), HNO_3 (11.3 μm), H_2O_v (6.4 μm–7.3 μm), and NO_2 (6.2 μm), and applied these observed atmospheric constituents to the study of photochemistry, radiation, and dynamics in the stratosphere and mesosphere (Gille and Russell, 1984). Measurements of water vapor profiles with a vertical resolution of 5 km (version 5) were retrieved from the channel centered at 6.9 μm over latitudes 64°S to 84°N, and have an accuracy when compared to correlative balloon measurements of 14%, which is within the error bars of the LIMS measurements (Russell et al., 1984).

A complete zonal picture of water vapor in the lower stratosphere obtained by LIMS showed the existence of a hygropause extending from the tropics to the mid-latitudes (to approximately 40 degrees) Russell et al. (1984). When the SAGE II data product became available over a half decade after the LIMS data (version 5) highlighted the global lower stratospheric water vapor features, SAGE II provided verification of a well defined hygropause and increasing water vapor mixing ratios with altitude in the tropics (Chiou et al., 1993).

SAGE II data showed a larger water vapor systematic bias when compared to LIMS, which was separated in time by less than a decade. When both LIMS and SAGE II were compared to the Spacelab 3 Atmospheric Trace Molecule Spectroscopy (ATMOS) data, SAGE II water vapor exhibited better agreement with ATMOS, implying that LIMS biases in mixing ratio and hygropause location are real and need to be taken into account when comparing LIMS data to other data sets (Chiou et al., 1993). There is also a high latitude bias in the LIMS data showing a wetter lower stratosphere at high latitudes than that seen in the SAGE II data (Remsberg et al., 1984).

Recently, a new version of the LIMS algorithm (version 6) was used to process the water vapor profiles, giving a better knowledge of the spacecraft altitude. This provided an improvement in the temperature profiles and the registration of the water vapor radiances with pressure (Remsberg et al., 2009). These improvements provide a more accurate measurement (approximately 26% error compared to approximately 40% error for the lower stratosphere) of water vapor from 3 hPa to 100 hPa. The improvements from version 5 (V5) to version 6 (V6) include a different temperature dependence model which improves the O_2 interference line in the H_2O_v channel, leading to an improved tropical lower stratospheric water vapor retrieval, and better pointing knowledge and jitter corrections which improved the latitude spacing from 4 degrees to 1.6 degrees. Additional refinements to the algorithm improved the

vertical resolution for H_2O_v to 3.7 km and improved resolution of the water vapor ratios in the upper stratosphere (methane oxidation region) and the mid-latitude lower stratosphere. The LIMS V6 zonal mean water vapor compares well with the Aura Microwave Limb Sounder (MLS) Version 2.2 zonal water vapor, agreeing to within 10% of each other despite the 26-year separation in the data sets (Remsberg et al., 2009).

This study will use the LIMS V6 zonal seasonal water vapor from approximately 3 hPa to 100 hPa to provide an extension to the climatological data record in seasonal water vapor in the stratosphere since 1978/1979 as seen in the SAGE II water vapor data record (1986–2005).

2.1.3 MLS

The Earth Observing System (EOS) Microwave Limb Sounder (MLS) instrument was launched on the Aura satellite on July 15, 2004. It is an updated and much improved version of the Upper Atmosphere Research Satellite (UARS) MLS instrument launched in 1991. Aura MLS data provides measurements of the dynamical tracers (e.g., water vapor) and chemical composition of the stratosphere, measurements of trace gases in the upper troposphere, and global coverage (98° inclination Sun-synchronous orbit) (Livesey et al., 2005). The instrument employs seven line-of-sight, limb-sounding sensors using the technique of high frequency microwave radiometry to measure vertical profiles of trace gases and atmospheric composition approximately every 25 seconds (Livesey and Read, 2000; Read et al., 2007). The data products are retrieved from measurements of five spectral bands centered near frequencies 118 GHz (temperature and pressure), 190 GHz (H_2O_v, HNO_3), 240 GHz (O_3 and CO), 640 GHz (N_2O, HCl, ClO, HOCl, BrO, HO_2 and SO_2), and 2.5 THz (OH) over 37 pressure levels from 1000 hPa to 0.001 hPa (Schoeberl et al., 2006; Waters et al., 2005).

Since MLS uses microwave wavelengths, the measurements are largely unaffected by cirrus clouds and aerosols. Thick clouds, however, will affect the radiance measurements (Livesey et al., 2007; Lambert et al., 2007). For the present analysis, quality flags are scanned prior to averaging monthly means to eliminate data that has been contaminated by thick clouds. Averaging also takes into account the logarithmic nature of the water vapor profile as specified by Livesey et al. (2007). The vertical resolution for water vapor variations are from 1.5 km at about 300 hPa to 3.5 km at 4.6 hPa. Level 2 processing using version 2.2 of the MLS algorithm represents an improved water vapor product from the earlier 1.5 version.

Vertical profiles of water vapor from the Aura MLS instrument are available for August 8, 2004 to the present and provide a picture of the current state of the stratospheric water vapor that is useful for climatological comparison with LIMS (1978–1979) and SAGE II (1986–2005). The 12 month overlap between SAGE II and Aura MLS permits comparisons of water vapor for quantitative differences of regional and seasonal water vapor.

This study uses the Aura MLS zonal and seasonal mean water vapor product to compare features seen in the SAGE II zonal seasonal water vapor product for the 2005 austral spring season. Aura MLS is also used to provide a back-end extension to the climatological changes seen since 1978/1979.

2.1.4 MERRA Data

The Modern Era Retrospective-analysis for Research and Applications (MERRA) data set is supplied by the Global Modeling and Assimilation Office at NASA Goddard Space Flight Center. The MERRA data products use the GEOS-5 atmospheric data assimilation system to collect and combine observations acquired over the satellite era into a synthesized climate-quality data set (Rienecker et al., 2011). Currently the MERRA data set extends from 1979 to the present and includes an extensive list

of meteorological products that can be accessed through NASA Goddard Space Flight Center, GMAO (2012) at http://gmao.gsfc.nasa.gov/research/merra/intro.php. This study uses the analyzed 3D Zonal Uwind, the assimilated (model generated) 3D Ertel's Potential Vorticity, and the assimilated 2D tropopause temperature.

2.1.5 Meteorological Data

NCEP reanalysis data (Kalnay et al., 1996) is used as a proxy for the location of the sub-tropical jet and therefore the poleward edge of the Hadley circulation. The core of the jet, and therefore the location of the poleward edge of the Hadley cell, is inferred from the zonal maximum Uwind component and will be useful as a widely-published and well-characterized context for the MERRA data product. Initial analysis of the sub-tropical jet was performed using the NCEP Uwind product to have a comparison with the SAGE II version 6.2 ancillary data, which uses NCEP pressure information in the data retrieval algorithms. Future SAGE II versions will use the MERRA data products.

2.2 Analysis Domains

For this study, the zonally averaged characteristics of the stratosphere are analyzed for seasonal water vapor variations and sub- and extra-tropical jet movement. SAGE II data are binned in 10-degree zonal latitude bins with a vertical resolution of 0.5 km in altitude. For the purposes of this study, which is concerned with the water vapor variations in the lower stratosphere, the altitude ranges used in analyzing SAGE II data will be confined to between 10 km and 35 km. This region bounds the hygropause from the equator to the polar regions of the globe.

LIMS and MLS water vapor analyses uses zonal bin sizes of 4 degrees in latitude with an altitude resolution of about 3.7 km for LIMS and about 2.5 km for MLS. Comparison with SAGE II water vapor is qualitative with explanations detailing how differing zonal bin sizes affect the qualitative interpretation.

Wherever possible, SAGE II monthly data are used as available in the zonal regions of interest. Seasonal data are only used when all three months of that season are available in the zonal regions under analysis. This does reduce the analysis sample size, however it provides more confidence in the seasonal means.

2.3 Statistical Treatment

Errors in the estimations of the monthly means are calculated using the weighted mean uncertainty equation specified in Bevington and Robinson (2003). Best fit linear regression analysis uses the monthly means and weighted errors of the monthly means to provide best fit slope, intercept, and the coefficient of correlation as outlined in Press et al. (1993). Statistical analysis includes calculating the 95% confidence bands of the linear regression best fit line using the Working-Hotelling $1-\alpha$ confidence band outlined in pages 40–63 from Kutner et al. (2005).

CHAPTER III

DECADAL VARIATIONS OF THE STRATOSPHERIC WATER VAPOR SEEN BY SAGE II

3.1 Water Vapor Comparisons

The SAGE II data product provides a unique opportunity for looking at decadal variations in stratospheric water vapor associated with large scale atmospheric circulation changes over the last three decades. Such inferences in the changes of the large scale circulation and stratospheric water vapor have made use of the combination of HALogen Occultation Experiment (HALOE) and radiosonde (Randel et al., 2004, 2006; Rosenlof and Reid, 2008) water vapor data from the early 1990s to the mid 2000s. The SAGE II water vapor data coverage extends from the mid to late 1980s up to the mid 2000s, highlighting even longer-term variations in the lower stratospheric water vapor. The LIMS (1978–1979) and MLS (2005–present) vertical profiles of water vapor in the stratosphere can be included to further extend the observations of climatology in the stratosphere. Qualitative comparisons of the SAGE II water vapor data with HALOE, LIMS, and MLS provide a record of water vapor variation in the stratosphere from the late 1970s to the present, which highlights a multi-decadal, dynamically changing stratosphere and has provided a rich area of active research in the mechanisms associated with the changes in the stratospheric water vapor.

3.1.1 SAGE II and HALOE Water Vapor Data

Figure 3.1 shows the SAGE II monthly mean water vapor data between 5°S–5°N for the contemporaneous, smoothed HALOE water vapor data originally published in Rosenlof and Reid's 2008 paper. Although the SAGE II data has many coverage gaps

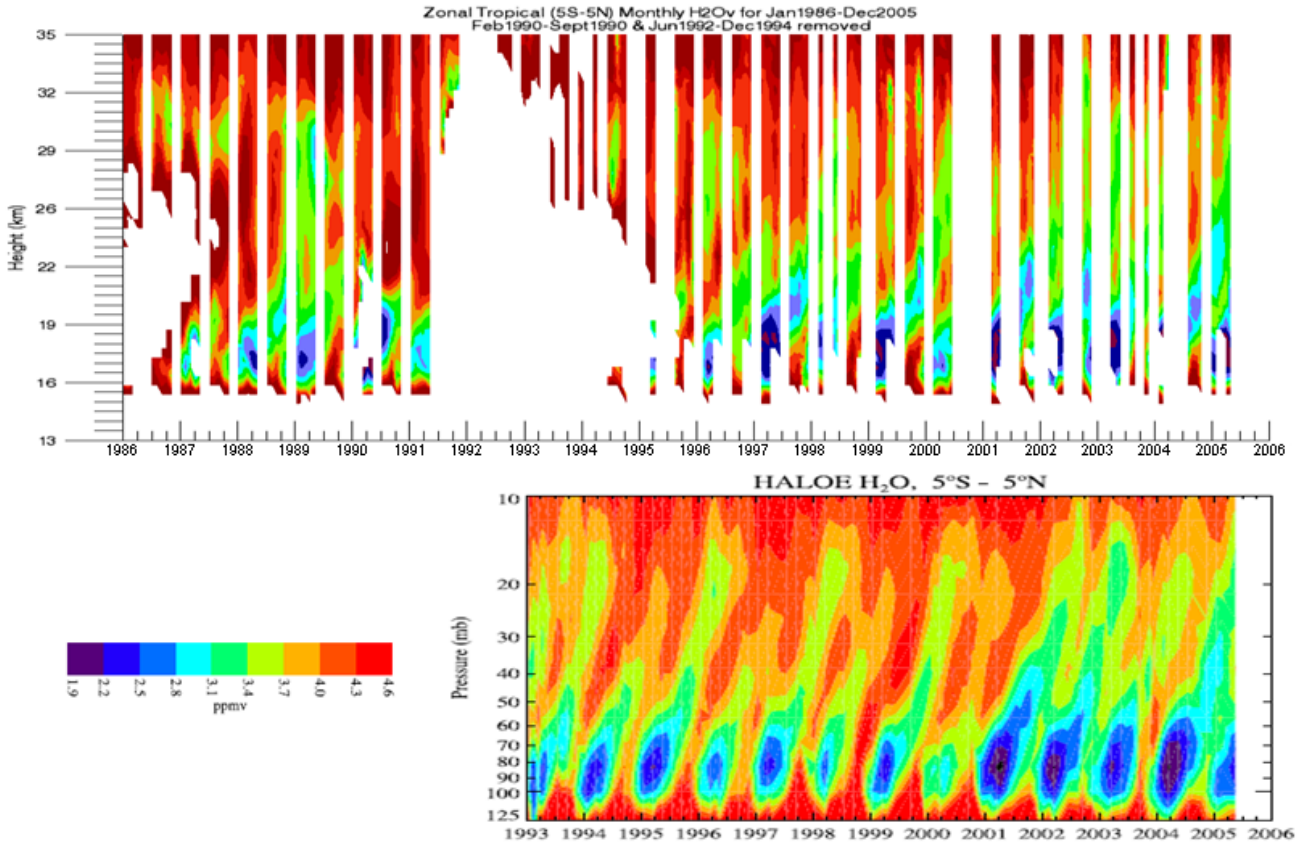

Figure 3.1: Comparison of the monthly water vapor mixing ratio between HALOE and SAGE II. The HALOE plot (Rosenlof and Reid, 2008) and SAGE II plot show the 5°S–5°N zonal region with the tape recorder apparent in both plots. The SAGE II data have a slightly drier bias when compared to the HALOE data. The colors and ppmv values used in the SAGE II plot were designed to mirror those used in the published HALOE plot. The two time series are aligned to allow vertical comparisons of time related water vapor.

in the tropical monthly record over the 20-years from 1986 to 2005 along with gaps from aerosol interference, the tropical tape recorder pattern is qualitatively similar to that seen in the HALOE data as published by Rosenlof and Reid (2008). Variations in zonal mean water vapor averaged over 5°S–5°N are clearly seen as water vapor moves from the lower stratosphere to the middle stratosphere over a time period of approximately 12 months as first described by Mote et al. (1995). Within the SAGE II data set, the tape recorder effect can be seen from the mid to late 1980s with slightly higher water vapor content from that seen in HALOE. Rosenlof and Reid (2008) also called attention to higher stratospheric water vapor in the mid to late 1990s as compared to the early 1990s and the 2000s. The increasing water vapor signal in the late 1990s stratosphere seen in the HALOE data set is mirrored in the SAGE II data set at certain latitudes and altitudes, and will be shown in Section 3.2. A comparison of the SAGE II zonal water vapor with two additional data sets that bookend the SAGE II data will extend the knowledge of the changing state of the lower stratosphere over 20-plus years.

3.1.2 SAGE II, LIMS and MLS Water Vapor Data

To qualitatively extend the water vapor record to validate long-term variations in the structure of stratospheric water vapor, a non-overlapping time series of the early SAGE II water vapor record with the LIMS water vapor data set is used as a representative extension of the state of the stratosphere. A comparison of the later SAGE II water vapor record with MLS seasonal water vapor can further provide verification as to the state of the stratospheric water vapor at the end of the SAGE II data record. This improves confidence that the SAGE II water vapor product accurately tracks

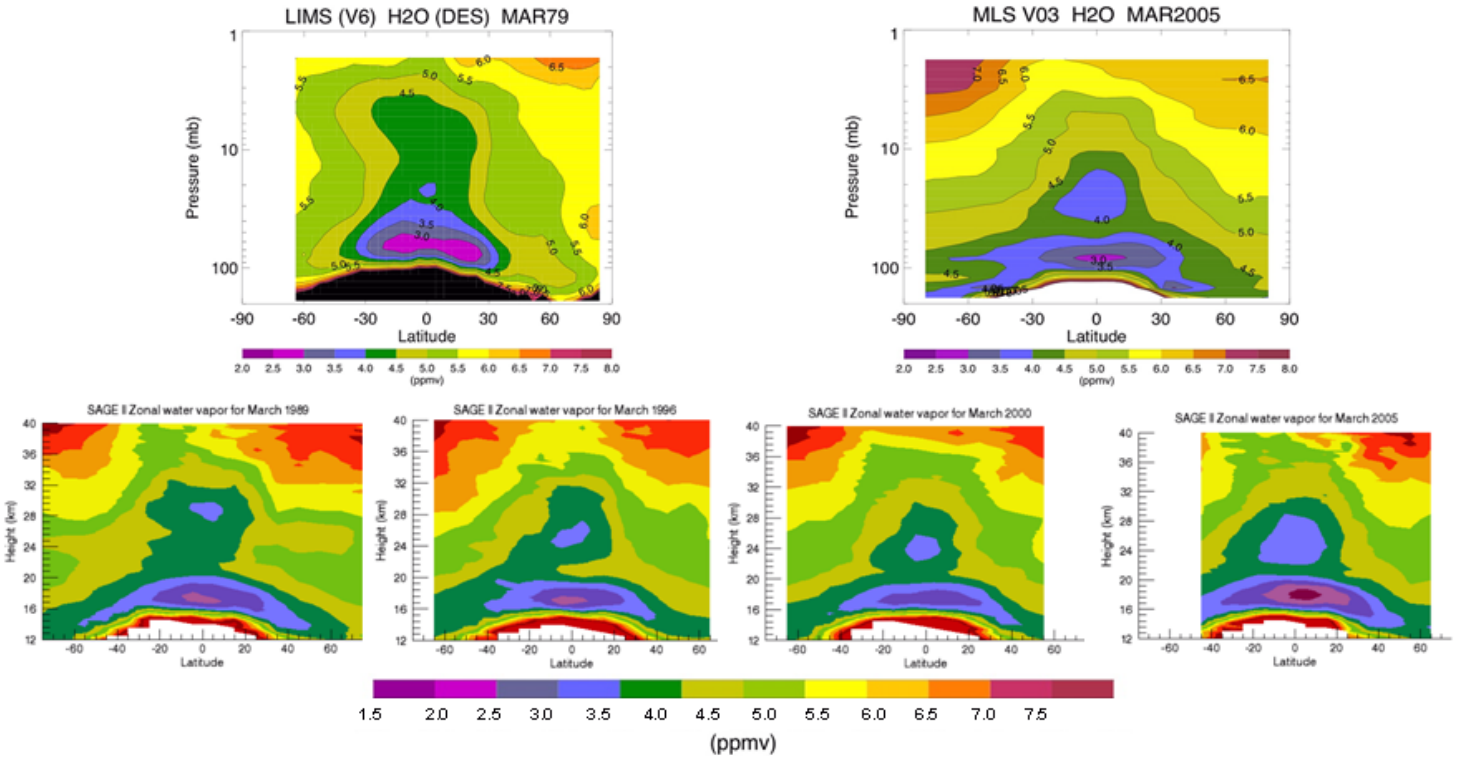

Figure 3.2: LIMS water vapor for March 1979 and MLS water vapor for March 2005 showing a change from a vertical stratification of the hygropause constrained primarily in the tropics and sub-tropical regions of the stratosphere to a more horizontal distribution of the hygropause extending to the poles. SAGE II monthly mean water vapor for March 1989, 1996, 2000, and 2005 show a progressive change in the stratospheric water vapor profile bridging the time frames of the LIMS and MLS data sets.

the monthly variations of the stratospheric water vapor over the 20-year record. Figure 3.2 shows contour plots of the March 1979 LIMS and March 2005 MLS water vapor, which are seasonally representative months and of the same approximate Quasi-Biennial Oscillation (QBO) phase as shown in the Freie Universität Berlin (2012) record, http://www.geo.fu-berlin.de/en/met/ag/strat/produkte/qbo/index.html.

Figure 3.2 also shows the SAGE II zonal water vapor data progressively changing pattern in the March monthly data from 1989 to 1996 to 2000 to 2005 and provides a bridge between the LIMS and MLS data sets, in the same approximate QBO phase. From Figure 3.2 it is apparent that a change has occurred in the lower to middle stratosphere over the last 25 years (1979 to 2005) where both the structure and abundance of water vapor progressively changes over this multi-decadal time frame. The tropical middle stratospheric (10 mb or ∼30 km) water vapor mixing ratio was drier in the early part of this study but increased in both the SAGE II and MLS records. This early record of drier air is confined to the tropical and sub-tropical region within an altitude range from the tropopause to the middle stratosphere, can still be seen in the SAGE II data (March 1989) ten years after LIMS measurements. The MLS (March 2005) and the later SAGE II data (March 2005) show a poleward spread of the driest air to a horizontal stratification, where the drier air extends from the tropics to the high latitudes in the lower stratosphere, near the end of this multi-decadal record. This change from a vertically deeper penetration of drier air into the middle stratosphere in the tropics, to a shallower but poleward spread of drier air indicates a possible change of the slower Brewer-Dobson circulation and the stronger poleward movement of air parcels in the lower stratosphere at or just above the hygropause into the mid-latitudes. This possible circulation change, along with other atmospheric changes that might explain the changes observed, will be investigated further in Chapter 4.

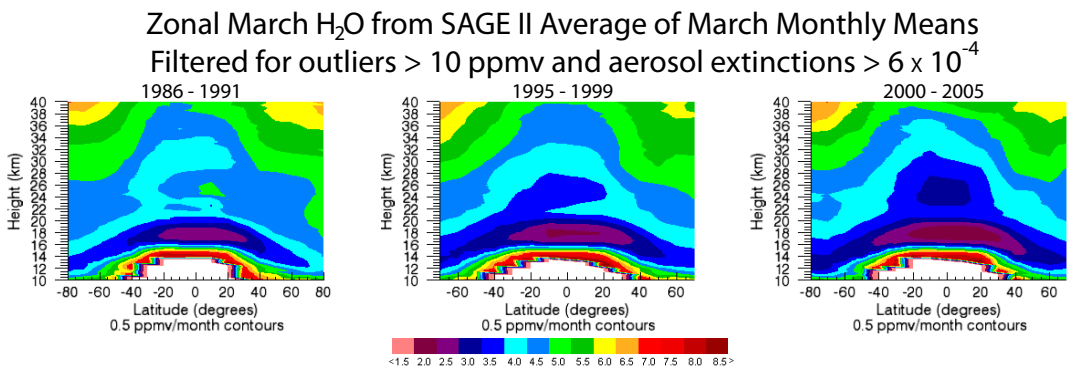

Figure 3.3: SAGE II sub-decadal average water vapor for March monthly means divided into three sub-decadal time frames, 1986–1991, 1995–1999, and 2000–2005.

3.2 SAGE II Water Vapor Signals

The monthly mean water vapor minimum or hygropause is located a few kilometers above the tropopause (Kley et al., 1979) and is formed by a combination of tropopause temperature fluctuations and atmospheric circulation patterns across the tropopause where the "cold trap" mechanism dehydrates the air that enters the lower stratosphere (Holton and Gettelman, 2001; Bonisch et al., 2010), providing a zone of minimum water vapor above the troposphere (Fueglistaler et al., 2009). Figure 3.3 shows the global zonal lower stratospheric water vapor retrieval during March for three sub-decadal segments (1986–1991, 1995–1999, and 2000–2005). The plots show a progressively poleward expansion of a drier hygropause from the period of 1986–1991 to that of 2000–2005. A progressive drying of the hygropause region was also reported by Read et al. (2004) based on the MLS data during the period from 1991–1994 and by Randel et al. (2004) based on the entire HALOE data product. This region of minimum water vapor (i.e., hygropause) can clearly be seen to change in the SAGE II March data from the three sub-decadal time frames, indicating that the region is getting drier. Whether this drying of the hygropause is caused by a temperature change at the tropical troposphere "cold-trap" along with other dynamic circulation changes in the atmosphere will be investigated in Chapter 4.

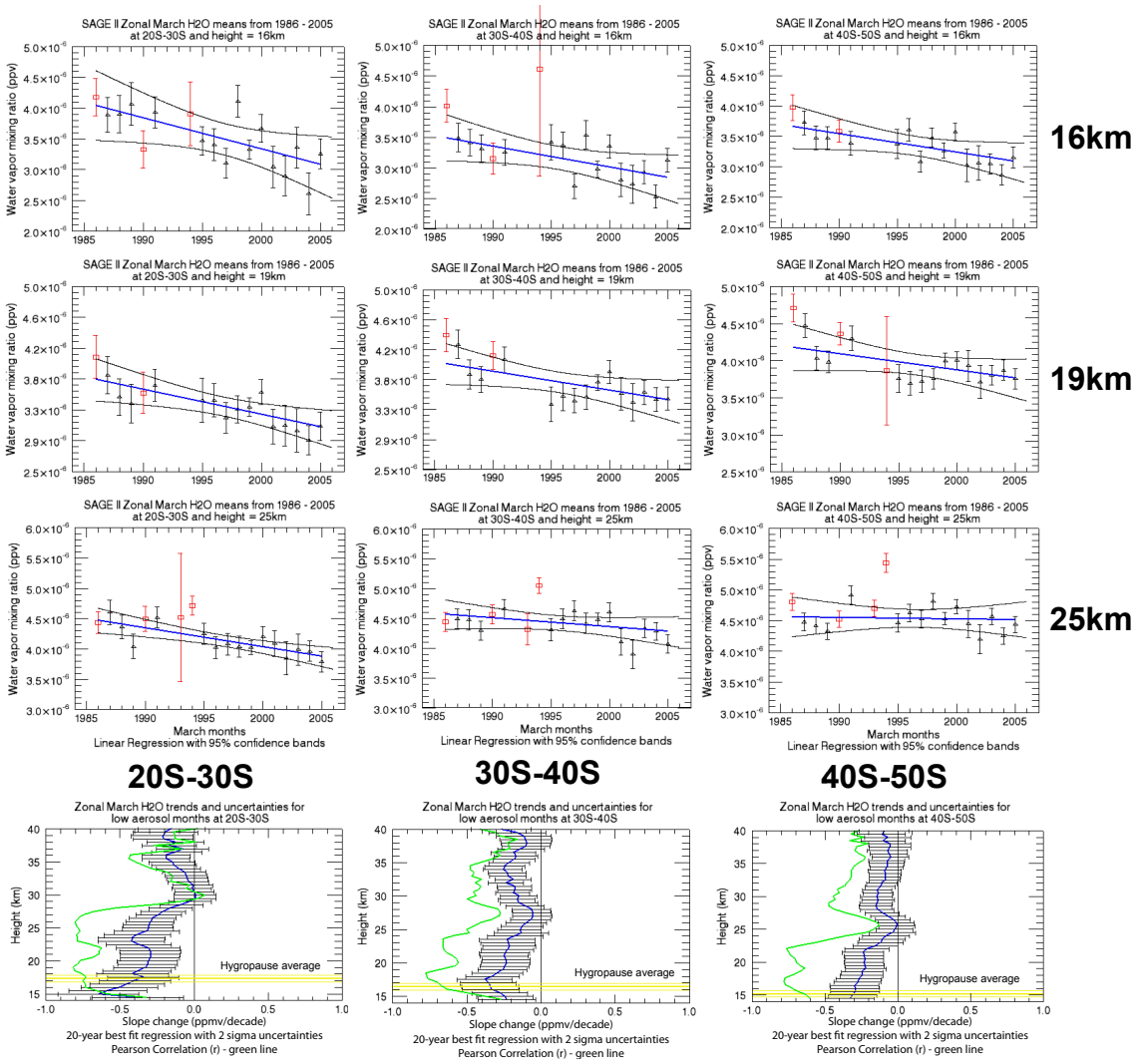

Figure 3.4: SAGE II zonal March monthly means at three heights (16 km, 19 km, & 25 km) in the stratosphere for three zonal latitude bins (20°S–30°S, 30°S–40°S, & 40°S–50°S) in the Southern Hemisphere from 1986–2005. Linear regression analysis (blue line) is included to show the long-term change in the water vapor record as seen by SAGE II. High aerosol years are represented in red and are not used in the linear regression analysis. Bottom plots represent the best fit linear regression slope as a function of altitude with the average height of the H_2O_v minimum (hygropause) shown in yellow for each latitude bin. Pearson r correlations (green line) of the linear regressions are also included in the trend plots.

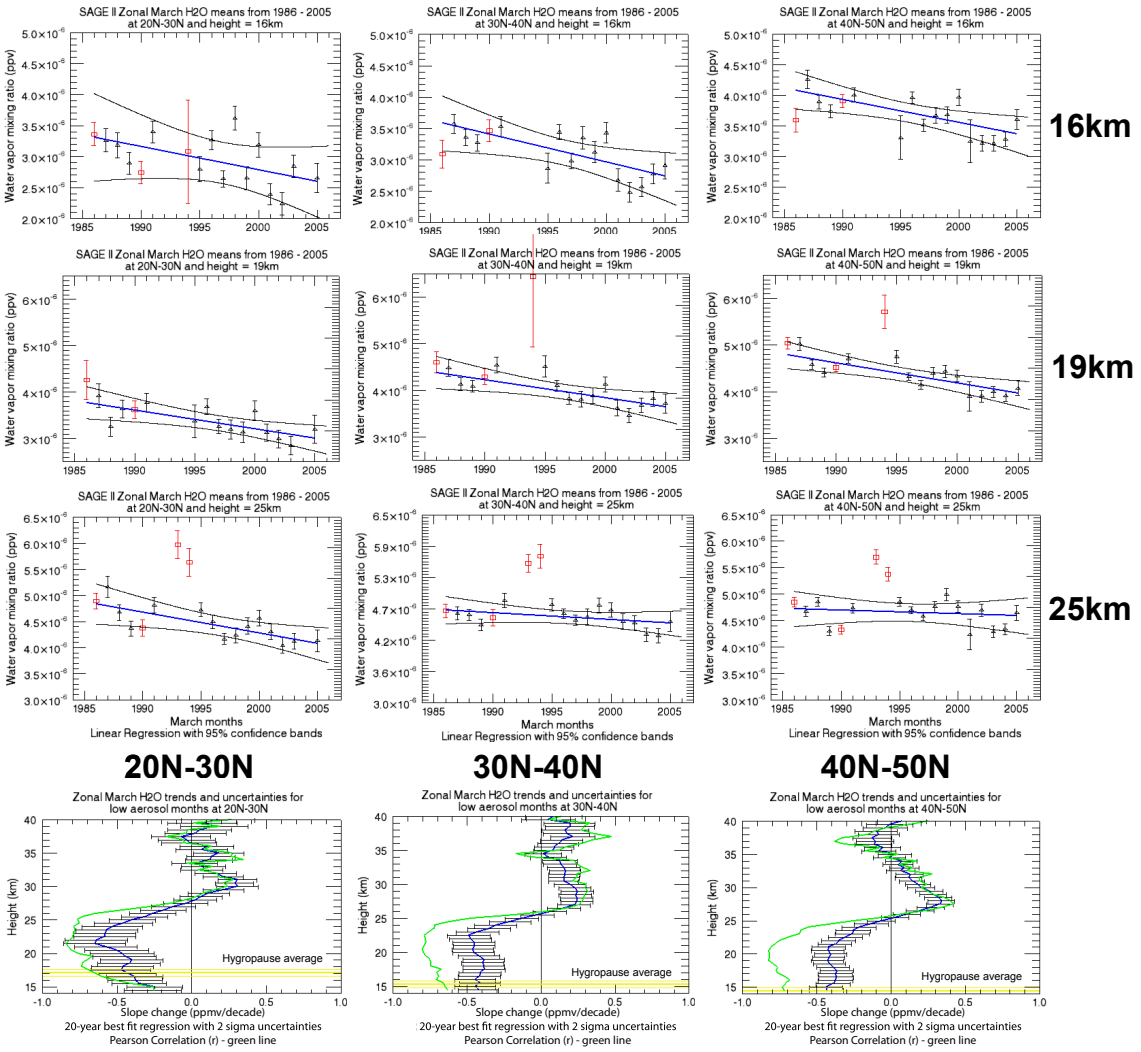

Figure 3.5: SAGE II zonal March monthly means at three heights (16 km, 19 km, & 25 km) in the stratosphere for three zonal latitude bins (20°N–30°N, 30°N–40°N, & 40°N–50°N) in the Northern Hemisphere from 1986–2005. Best fit slopes with 2-σ uncertainty between the altitudes of 14 km–40 km are represented in the bottom three trend plots. This is the same as in previous Figure 3.4 but for the Northern Hemisphere mid-latitudes.

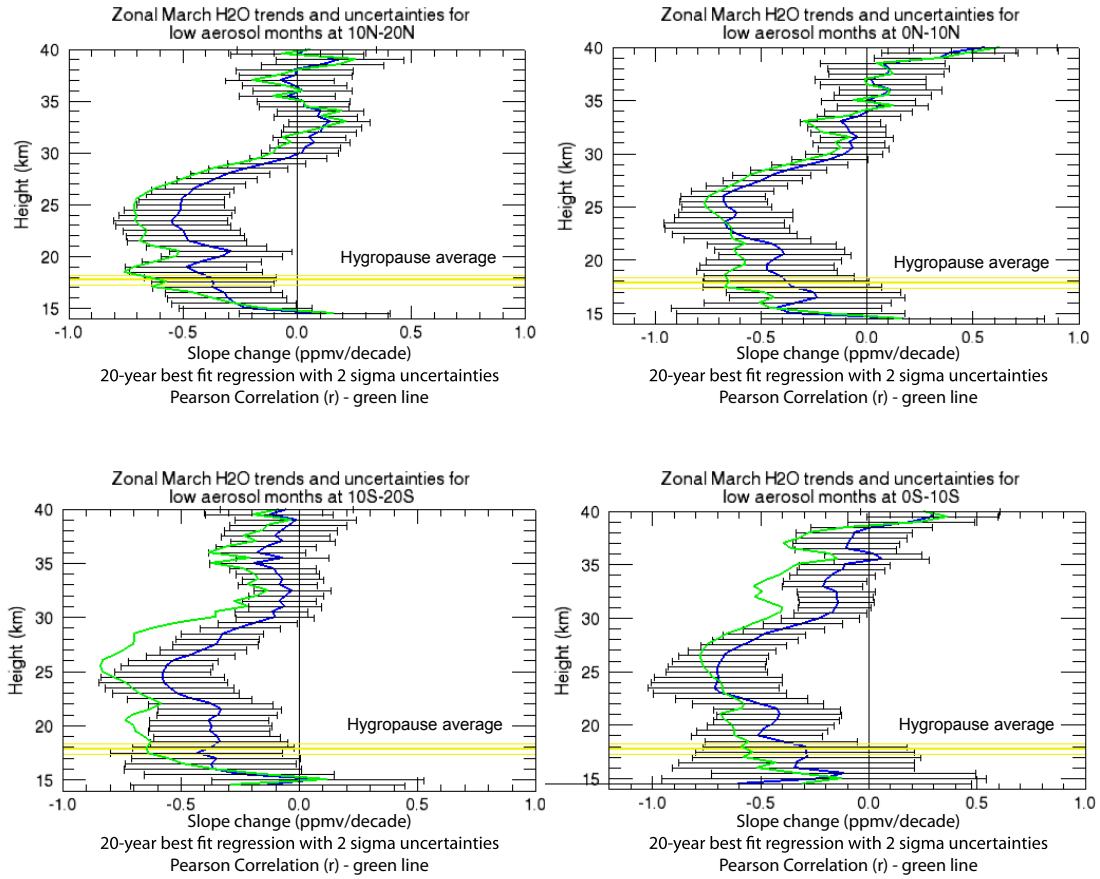

Figure 3.6: Tropical region water vapor trends and the 2-σ uncertainty on the linear regression as seen in the SAGE II water vapor data. High aerosol years (1986, 1987, 1990, 1992–1994) were not used in the determination of the best fit linear regression analysis. The average height of the H_2O_v minimum (hygropause) is shown in yellow for each latitude bin and the Pearson r correlation coefficient (green line) of the linear regressions are also included in the trend plots.

The SAGE II water vapor data was more comprehensively analyzed for decadal variations in each zonal latitude bin at heights from 14 km to 40 km. Figures 3.4, 3.5, and 3.6 show the decadal variations of the lower stratospheric water vapor in March over the southern, northern, and tropical zones, respectively, over the SAGE II 20-year time period. The mean Southern Hemisphere mid-latitude water vapor during March at three discrete altitudes along with the linear regression plots with 95% confidence bands that show the 20-year trends and 2-σ uncertainty on the regression slopes for the altitudes from 14 km to 40 km are shown in Figure 3.4. The uncertainties on

the linear regression slope incorporate the measurement error of the monthly means at each altitude. The years of 1986, 1990, and 1992–1994 with high aerosol are not used when calculating the linear regression slope but are shown in the plots as red squares with their reported measurement uncertainties on the monthly mean water vapor at each altitude. The hygropause is represented by an average of the water vapor minimum calculated from the SAGE II March monthly minimum water vapor abundance with an uncertainty delta of half a kilometer (yellow lines on the regression plots). The SAGE II data shows a statistically significant drying trend in the Southern Hemisphere sub-tropical/mid-latitude lower stratosphere for the March season at all latitudes bins from 20°S–50°S. Figure 3.5 shows the plots and trends for the Northern Hemisphere sub-tropical and mid-latitude zonal regions with similar long-term drying trends above the hygropause over the 20-year record. The lower stratosphere was wetter in the 1980s compared to the 1990s followed by a significant drop in the water vapor abundance after 2000. The discontinuity that occurred after 2000 is conspicuous below 25 km and has been documented by Randel et al. (2004) using the HALOE data set. Figure 3.6 shows the trends for the tropical region (20°N–20°S) in 10-degree zonal bins. Aerosol from the volcanic eruptions in 1986/1987 affected the tropical region over a longer period of time necessitating the removal of the March 1987 water vapor signal from the linear regression analysis. This tropical bias on the March 1987 data is consistent with the location of high aerosol extinctions shown in Figures 2.3 and 2.5, which document aerosol effects on the water vapor data in the tropical regions. Removal of the March 1987 tropical data still yields a significant and valid dehydration trend over the long-term time frame.

The variations seen in the SAGE II water vapor 20-year data record at altitudes below 25 km are between -0.25 to -0.7 ppmv decade^{-1} or between -0.07% to -0.15% decade^{-1} in the tropical and mid-latitudes at various altitudes. A large part of this decreasing long-term variation in the stratosphere can be attributed

to the drop in water vapor between the 2000 and 2001 seasons as documented by Randel et al. (2006) where they reported an overall global water vapor decrease of -0.4 ppmv after 2000 as seen by HALOE. Randel et al. (2006) reported that prior to the year 2000, the HALOE data did not show a significant change in the stratospheric global (60°S–60°N) mean water vapor from 1992–1999. Oltmans et al. (2000) reported a regional North American water vapor increase of 0.05 to 0.07 ppmv yr^{-1} over Boulder, Colorado and Washington DC using balloon-borne frost-point hygrometers up to the year 2000. This was inconsistent with the HALOE water vapor data which showed no change or even a decrease below 20 km in the same region. A reanalysis of the Boulder, Colorado balloon-sonde data performed by Scherer et al. (2008) corrected the linear trends from 1981–2006. This reduced the previous increasing trend in water vapor by 40% and indicated that the trend was not significant at the 95% confidence interval. In contrast, analysis by Scherer et al. (2008) showed a significant negative trend in the lower stratosphere for 1992–2005 in the HALOE data of -0.04 ± 0.02 ppmv yr^{-1}, which is consistent with the value seen by SAGE II in the latitude bin 30°N–40°N below 25 km (Figure 3.5). Solomon et al. (2010) looked at the regional North American mid-latitudes and reported a slight increase in lower stratospheric water vapor in the 1990s from both HALOE and balloon-sondes over Boulder, Colorado on the order of 0.5 ppmv decade^{-1}. SAGE II data shows an increasing variation below 20 km in the 30°N–40°N zonal latitude bin for 1995–1999 (not shown), however this analysis is not statistically significant because of the small number of data samples available for linear regression.

The decadal trends are most conspicuous in the lower stratosphere below 25 km in the mid-latitudes with little or no changes seen in the upper stratosphere above 25 km. The attribution for this dehydration is likely the transport of water vapor across the tropopause as opposed to changes in atmospheric circulation above 25 km. To further examine this decadal variation in the lower stratospheric water vapor with

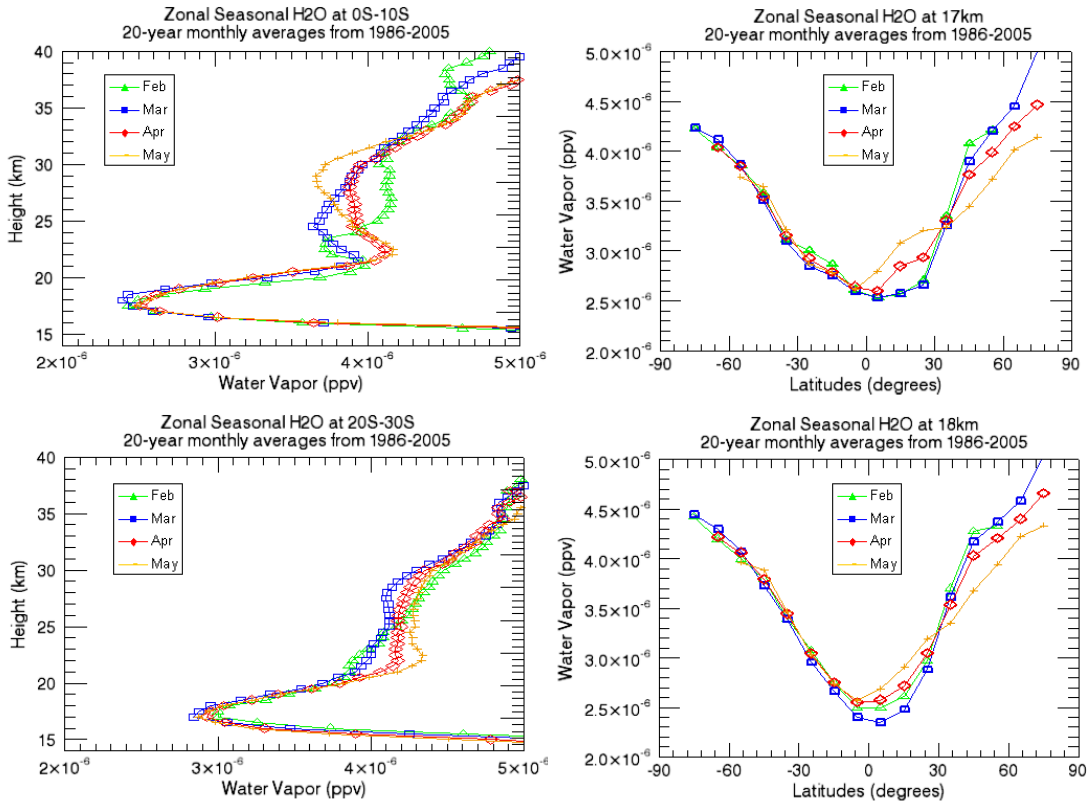

Figure 3.7: SAGE II seasonal 20-year means for Feb–May 1986–2005. March is the driest month for most of the latitudes in the 20-year record. The seasonal driest location is in the topics and sub-tropical latitudes at the altitude in those regions between 17 km–19 km (just above the tropopause).

an emphasis on the location for the initiation of the dehydration trend, this study examines the variations in the hygropause by analysis of the water vapor minima in the SAGE II data. The circulation changes associated with tropical broadening or the permeability of the sub-tropical transport barriers, which could account for decreases in water vapor in the lower stratosphere and hygropause over the 20-year record, are explored in Chapter 4.

3.2.1 Seasonal and Hygropause Analysis from SAGE II Water Vapor

From the previous section, the SAGE II 20-year water vapor data have shown that the lower stratosphere is getting drier for the time series of March monthly means. The tape recorder retrievals in the tropics seen in Figure 3.1 have both the HALOE

and SAGE II water vapor data showing a seasonal minimum water vapor signal in the boreal late winter/early spring months. Russell et al. (1993), Read et al. (2004), and Fueglistaler et al. (2005), using HALOE, MLS, and European Centre for Medium-Range Weather Forecasts (ECMWF) 40 Year Re-Analysis (ERA-40) data products respectively, have also shown that the seasonal water vapor minimum occurs in the months of February and March, and their corresponding boreal winter and spring seasons in the lower stratosphere. To pinpoint the seasonal month showing the lowest seasonal water vapor mixing ratio, the SAGE II 20-year monthly seasonal mean water vapor data for the months of February, March, April, and May is plotted in Figure 3.7. The full monthly mean annual cycle has been examined in this study, but only the driest seasonal months are shown for simplicity. The March 20-year seasonal mean has the lowest water vapor mixing ratio in almost all the zonal latitudes bins analyzed with a minimum at altitudes in the tropics and sub-tropics between 17 km–19 km. These observations of a seasonal minimum and the fact that the March months are well represented in the SAGE II data set over the entire 20-year operation of the instrument provides a data set that can be used to look at the decadal seasonal extreme hydration variations in the lower stratosphere.

The altitudes of the SAGE II water vapor mixing ratio minima, which define the hygropause, required determining the monthly minimum mixing ratio and the measurement error associated with that minimum mixing ratio for each event profile along with the tropopause height reported for each event. Then the mean and standard error in the estimation of each mean were calculated. This was done for all the events in each zonal latitude bin for each month in the 20-year SAGE II record. To ensure that the minimum value is a true minimum and not a termination of the event signal by sub-visual clouds, a check was performed to determine that the minimum water vapor value found is not the lowest altitude with a valid measurement in the event.

Additional filtering eliminated mixing ratio values below 0.5 ppmv and minimum values located below the tropopause. Once the event mixing ratio minima, measurement errors, altitude locations, and reported tropopause altitude were found in each zonal latitude bin, the monthly means were calculated for these four minima parameters in that event. The uncertainty calculation of the monthly minimum water vapor mean uses the usual weighted mean error equation from Bevington and Robinson (2003) to account for the variance in the measurement errors included in each minimum monthly mean.

Figure 3.8 shows the minimum water vapor for the entire 21-year record from SAGE II water vapor data with the volcanic aerosol events highlighted along with the minimum water vapor record with those high aerosol months removed. The low aerosol monthly minima show a drying over the 20-year record in the zonally averaged tropical and sub-tropical regions of the globe, with a significantly drier hygropause present in the tropics/sub-tropics for the month of March 2000, which is consistent with the results found by Randel et al. (2006) and Read et al. (2004). The El Chichon (17°N), Mt. Ruiz (5°N), and Mt. Pinatubo (15°N) eruptions produced aerosols that affected both hemispheres and erroneously enhanced the retrieved water vapor, producing higher mixing ratios than the average, while the Mt. Kelut (8°S) aerosols affected the tropics and Southern Hemisphere producing a smaller than average water vapor retrieval (Thomason et al., 2004). The months affected by these four major eruptions and seen in the aerosol extinctions (Figure 2.3) were removed when looking for monthly minima and long-term variations in the water vapor over the 20-year SAGE II data record.

A progressively drier zonal mean hygropause, for the March months, spanning the SAGE II 20-year record is seen over all zonal latitude bins extending to the poles (Figure 3.3). This increasing dehydration of the hygropause is most apparent in the tropics after March 2000, indicating that some transition occurred in the lower stratosphere

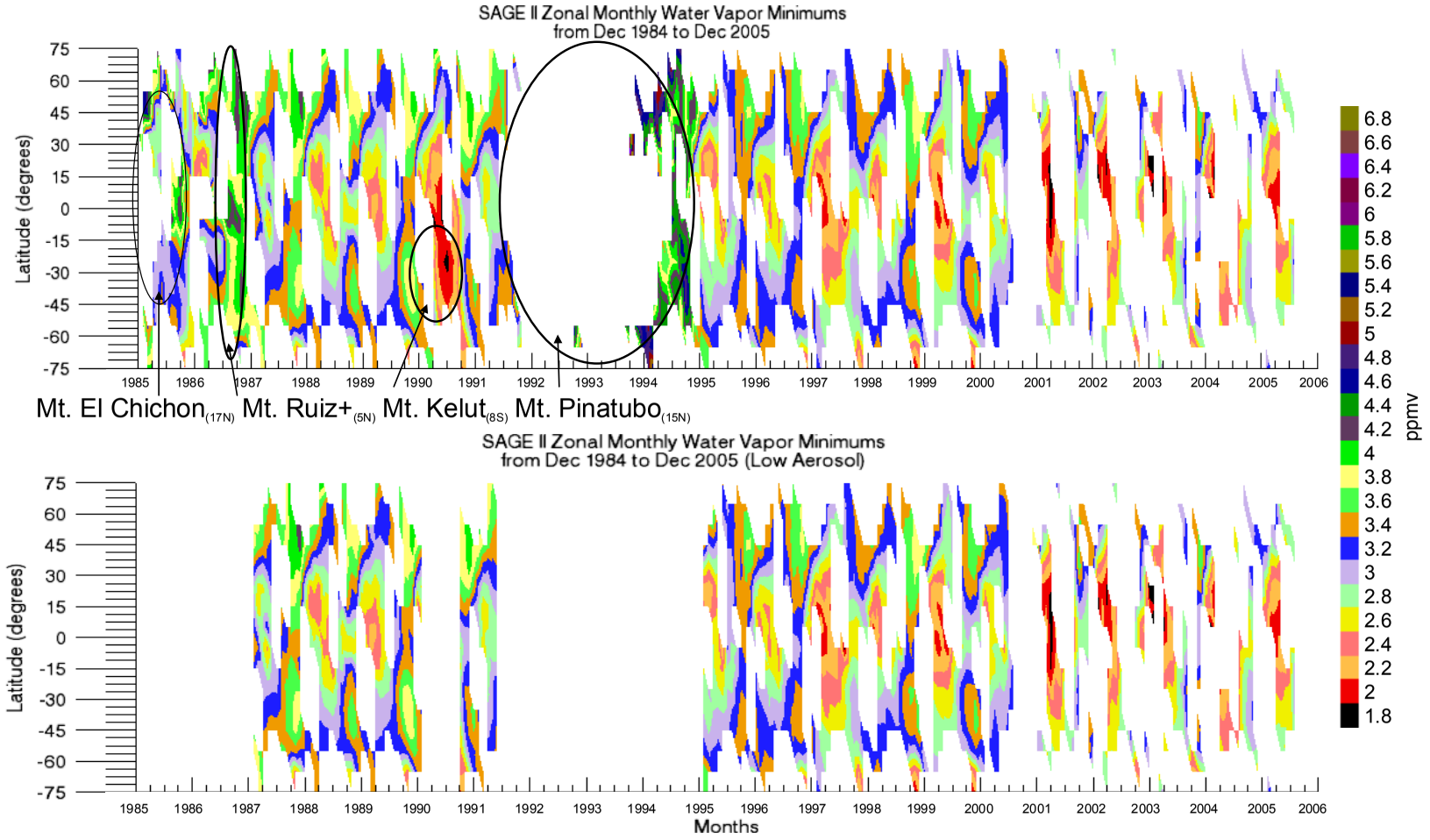

Figure 3.8: Zonal SAGE II monthly minimum water vapor values from December 1984–August 2005 before removal of the months where volcanic eruptions occurred (top) and after those months have been removed (bottom).

at that time which persisted through the end of the SAGE II data record (2005). The transition after 2000 has been linked to temperature and ozone changes that are a response to an increase in the Brewer-Dobson circulation (Randel et al., 2006, 2007, 2009; Garcia and Randel, 2008). Randel et al. (2006) showed a clear negative temperature anomaly in the tropopause temperature in the tropics beginning in 2000/2001, which would lead to increased dehydration of the lower stratosphere through the process of increasing "cold-trap freeze-drying" of the upwelling tropospheric water vapor (Brewer, 1949; Mote et al., 1995; Holton et al., 1995) detrained from deep convective storms and/or an increase in the mean upwelling circulation caused by a stronger Brewer-Dobson circulation. A more detailed look of the possible processes that could lead to a drier hygropause is provided in Chapter 4.

The 20-year March monthly minimum water vapor mixing ratios, the 20-year seasonal monthly minimum water vapor mixing ratios, and the monthly average of the hygropause height in the tropics, sub-tropic and mid-latitudes for March are shown in Figure 3.9. The overall trend in the water vapor minimum is negative primarily dominated by the contribution after the year 2000. By the end of the SAGE II data record, however, the water vapor minimum had not recovered to pre-2000 zonal mean levels from the tropics to the mid-latitudes. The top right plot in Figure 3.9 shows the seasonal SAGE II 20-year monthly means as a function of latitude. The March monthly means have the driest hygropause from the tropics to approximately 50°S and 50°N. The SAGE II data show a sharp decrease in the mean water vapor minima in the Southern Hemisphere high-latitude for the months of September, October and November. The September minimum mean in the 70°S–80°S zonal latitude bin, however, is a single sample from 1990, and the November mean in the same latitude bin is derived from 5 samples from 1995–1999. Vömel et al. (1995) and Nedoluha et al. (2002) documented this dehydration process in the southern polar region attributing it at and above the hygropause as the process of an air parcel

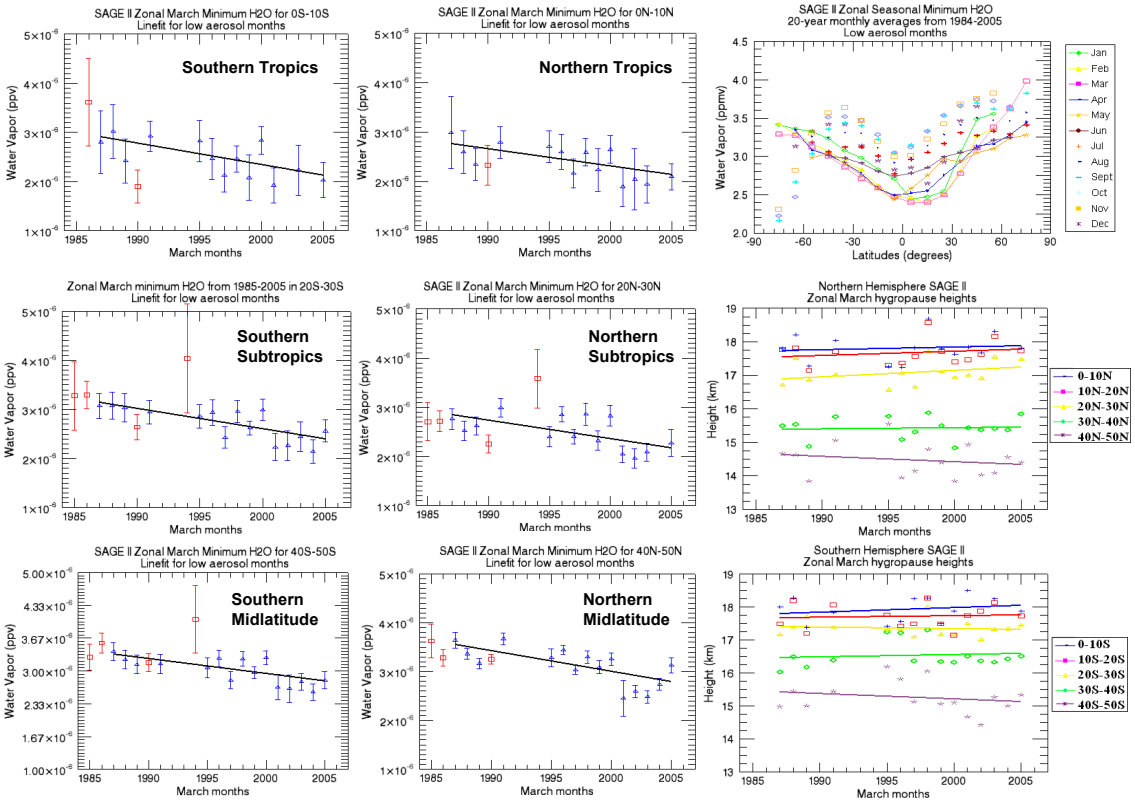

Figure 3.9: SAGE II zonal March minimum monthly means in the stratosphere for three zonal latitude bins (0°–10°, 20°–30°, & 40°–50°) in the Southern and Northern Hemispheres from 1985–2005. Linear regression analysis is included to show the long-term change in the water vapor record as seen by SAGE II. High aerosol years are represented in red and are not used in the linear regression analysis. The 20-year seasonal minima across all latitudes show March as the driest average month. The altitude location for the minimum March water vapor signal defines the hygropause and is shown at five latitude bins for both hemispheres (bottom right plots).

undergoing multiple dehydration events inside the polar vortex. Future studies, which are outside the scope of this thesis, will explore this high latitude dehydration in the Southern Hemisphere.

The bottom right panels of Figure 3.9 show the hygropause location over time for latitude bins in both hemispheres. All of the latitude bins show a relatively stable zonally averaged hygropause altitude from the tropics to the poles within the 0.5 km vertical resolution of the SAGE II water vapor product. The stable altitudes of the zonally averaged minimum water vapor over the 20-year analysis period points to a long-term stability in the vertical temperature profile of the zonal mean atmosphere. The relatively stable altitude of the zonally averaged hygropause and the decreasing water vapor record from 1986–2005 are consistent with trends found in other data sets of water vapor, temperature, and ozone measurements from HALOE (Randel et al., 2006; Garcia and Randel, 2008; Rosenlof and Reid, 2008; Solomon et al., 2010), SSU (Randel et al., 2009), balloon-borne frost point hygrometers (Rosenlof and Reid, 2008), and MLS (Read et al., 2004, 2008). To determine the possible causes of the drier hygropause during the 20-years of March seasonal changes, three mechanisms at the transport barrier in the tropics and sub-tropics between the troposphere and stratosphere are examined in the next chapter.

CHAPTER IV

VARIATIONS OF THE TRANSPORT BARRIER AND THEIR IMPACTS ON THE HYGROPAUSE

As discussed in Chapter 1, there are three possible pathways for moist tropospheric air transport into the lower stratosphere that could account for the variations seen in the lower stratospheric minimum water vapor retrievals from 1986–2005. The main region for transport of moist upper tropospheric airmass occurs in the tropics, where the "cold trap" at the tropical tropopause dehydrates the air mass that is ascending into the lower stratosphere. This region of seasonal transport can occur across the entire tropical region from the equator to the location of the sub-tropical jet where transport can occur diabatically driven by radiative heating in deep tropics or adiabatically across the tropopause fold near the subtropical jets following potential temperature surfaces. If the "cold-trap" at the tropical tropopause was decreasing, drier air would be transported into the tropical lower stratosphere and an increasing B-D circulation could then quickly move this drier airmass up into the middle stratosphere in the tropics and meridionally to the pole at the "tropical leaky pipe" location just above the tropopause. In addition, if the tropical region was expanding over time to the poles, the region for transport to and from the LS and UT would expand likely affecting the presence of water vapor in theses region.

To help explain the variations seen over the 20-year record in the SAGE II lower stratospheric water vapor and the hygropause, three proxy parameters in the region of the transport barrier between the troposphere and stratosphere are examined (Figure 4.1). The first analysis regards changes in tropical and sub-tropical tropopause temperatures for the seasons prior to the March annual minimum in water vapor. This

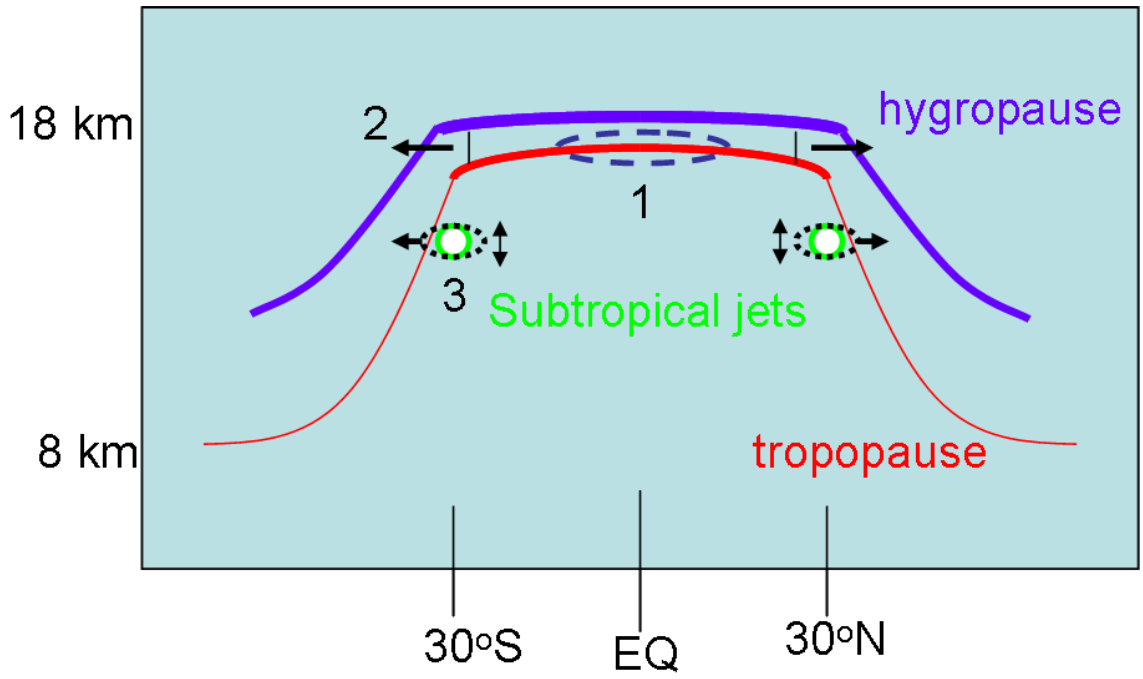

Figure 4.1: Schematic of the three transport barrier regions under investigation. The temperature of the tropopause at the tropics (1); zonal movement in the difference between the hygropause and tropopause altitude which is fairly constant at the tropics and subtropics would indicate tropical broadening (2); and movement and zonal variations in the subtropical/extra-tropical jet (3) could indicate changes in the transport barrier in these regions.

lag time accounts for the slow transport of air from the troposphere into the lower stratosphere as documented by Mote et al. (1995). The second analysis examines changes in the location of the hygropause relative to the location of the tropopause, which would indicate tropical broadening into the extra-tropics affecting the transport of water vapor into the lower stratosphere outside of the tropical latitudes. The third analysis looks at Ertel's Potential Vorticity (EPV or PV for short) and maximum zonal Uwinds to determine changes in the horizontal transport barrier at the location of the sub-tropical/extra-tropical jets for the season or months preceding the minimum water vapor signal.

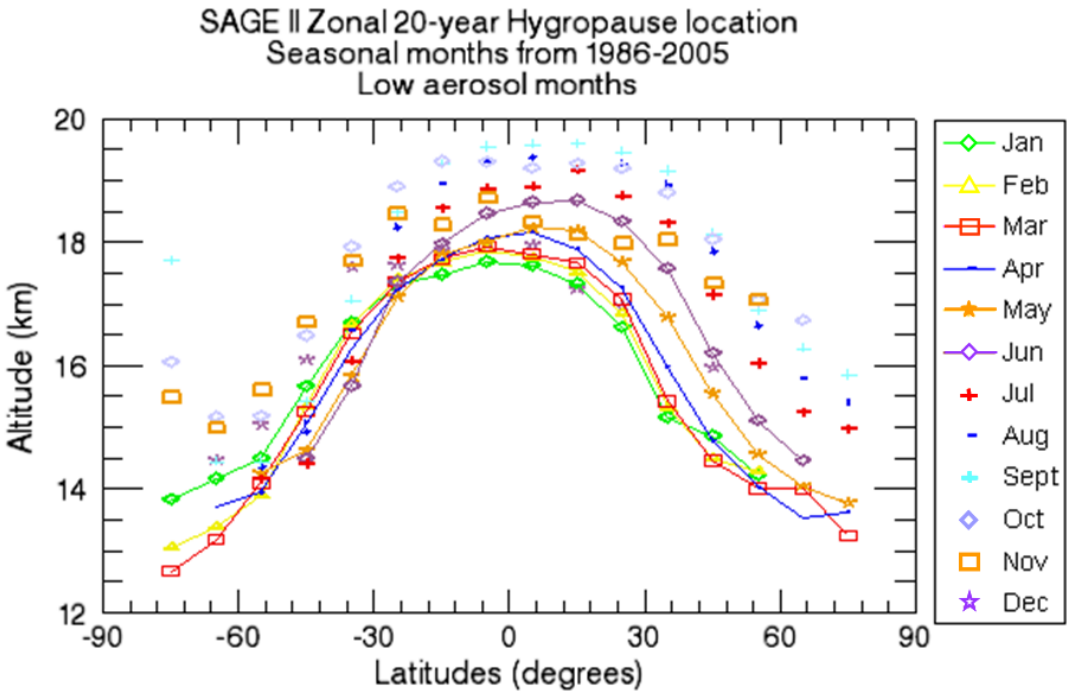

Figure 4.2: SAGE II 20-year (1986–2005) zonal seasonal mean of the hygropause location for the months of January through December.

4.1 Tropical Tropopause Temperature Analysis

To look at the processes giving rise to the dehydration of the hygropause over the last 25 years, recent studies have concentrated on the dynamical processes surrounding the Tropical Tropopause Layer (TTL) (Fueglistaler et al., 2009). The TTL is defined to be a wide region from 14 km to 18.5 km extending from the equator to 30 degrees in latitude for both hemispheres independent of season. It is interesting to note that the seasonal hygropause, found in the SAGE II water vapor data resides within the TTL during boreal winter and spring seasons but extends beyond the top range of the TTL for the boreal summer and fall seasons in the tropics (Figure 4.2). The TTL bounds the tropopause and the "cold trap" location above the tropopause. The "cold trap" region is where the dehydration of the moist tropospheric air parcels transitioning into the lower stratosphere in the tropics occurs (Fueglistaler et al., 2005; Liu et al., 2010;

Wright et al., 2011). Randel et al. (2004) has shown a correlation between colder tropopause temperatures and the decreased water vapor seen by HALOE after the year 2000. Since SAGE II water vapor data show that the March season is the driest season in the annual record, an analysis of the tropical tropopause temperatures prior to that seasonal minimum should have the lowest seasonal tropopause temperatures assuming that the dehydration of the stratospheric air parcels in the tropics is primarily a function of the "cold trap" mechanism. There should also be a trend towards colder tropopause temperatures to match the decreasing trend in the hygropause from 1986–2005. The tropopause temperatures were analyzed from the MERRA 2D data set, which can be downloaded from http://gmao.gsfc.nasa.gov/research/merra/intro.php (NASA Goddard Space Flight Center, GMAO, 2012).

The analysis of the tropopause temperatures from the MERRA data set shows that downward trends with Student's t-test significance greater than 95% in the discrete 0.5° latitude bins exist for December from **8°S–33°S** and 40°S–47°S, January from **28°S–17°N**, 40°S–50°S, 47°N–55°N, and 70°N–82°N, March from **10°N–12°N** and 38°S–45°S, and DJF from **23°S–16°N** and 42°S–50°S, with the latitudinal ranges within the TTL highlighted by **bold font**. The 20-year temperature changes in February, in each discrete 0.5° latitudinal bin, were not significant at greater than or equal to 95%. A significant decrease of the tropical tropopause temperatures within the TTL occurred during December and January (Figure 4.3), prior to March when drying of the hygropause was strongest. Thus, the decrease of the tropical tropopause temperature in January and February can explain a dehydration of the air across the transport barrier by the "cold trap" mechanism. As this colder, drier air moves both vertically with the Brewer-Dobson (B-D) circulation and along isentropic contour lines just above the tropopause, it is transported over time to produce a drier hygropause from the tropical region to the poles (Fueglistaler et al., 2005).

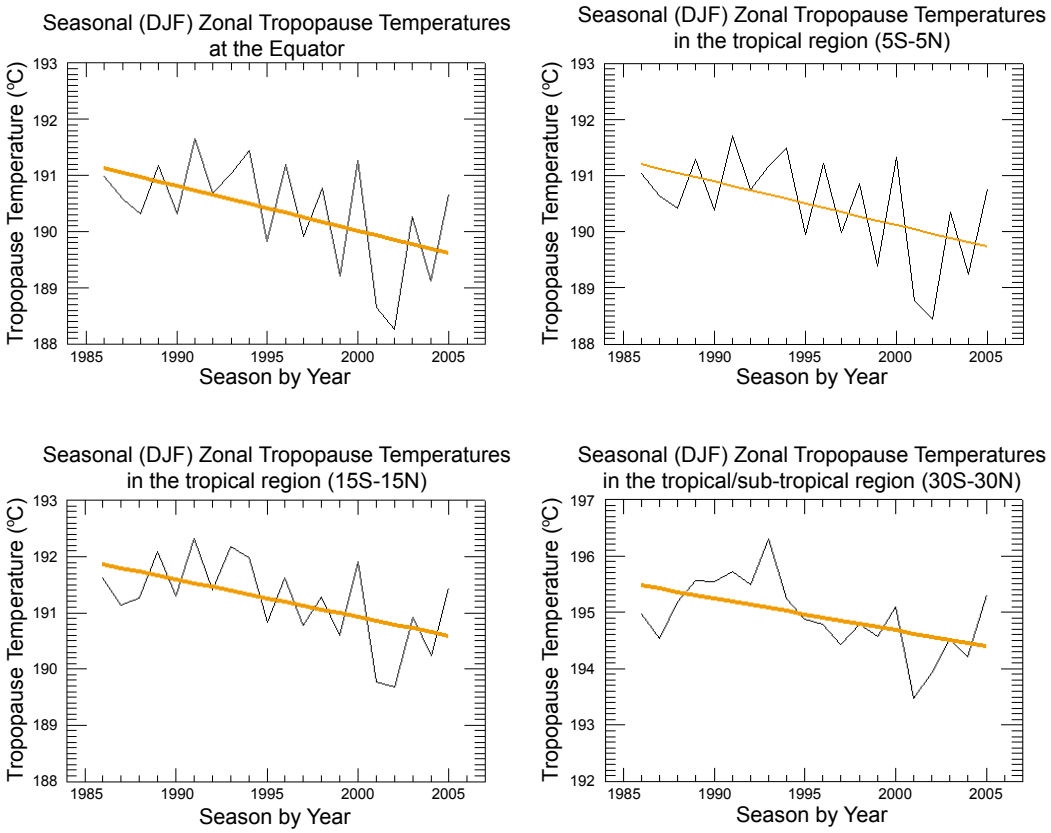

Figure 4.3: Zonal seasonal tropical tropopause temperatures for DJF in the TTL latitude bins. All DJF seasonal trends shown have a Student's t-test significance of 95%. The 15°S–15°N DJF seasonal trend is significant at 99%.

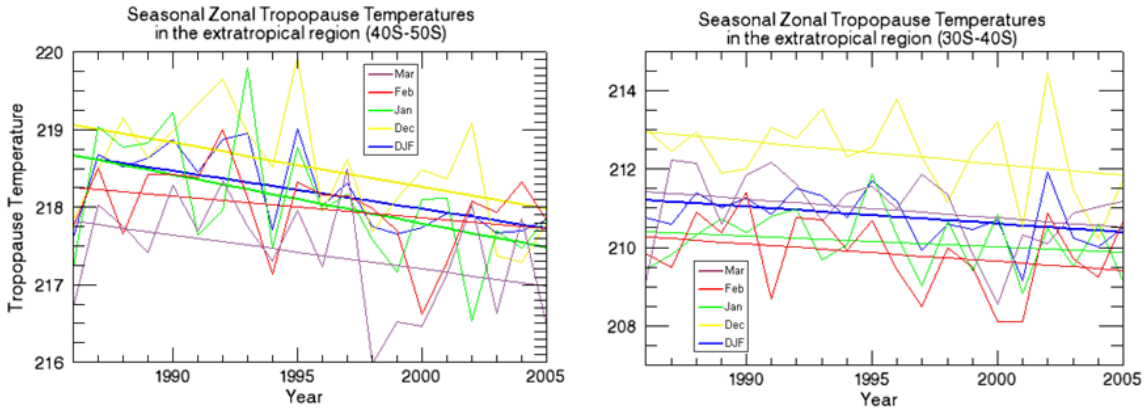

Figure 4.4: Seasonal (DJF) and monthly (Dec, Jan, Feb, and Mar) 20-year tropopause temperature changes at the zonal southern mid-latitude from 40°S–50°S and 30°S–40°S. The DJF (blue), Dec (yellow), and Jan (green) tropopause temperature changes are significant at greater than 95% for the 40°S–50°S zonal latitude, but only the DJF is significant at greater than 95% for the 30°S–40°S zonal latitude.

To investigate whether tropospheric air entering isentropically into the lower stratosphere at southern mid-latitudes outside the defined latitude range of the TTL can also be affected by the change in the tropopause temperatures, Figure 4.4 shows the MERRA tropopause temperature data at the 30°S–40°S and 40°S–50°S zonal latitude bin for the DJF season and the months of December, January, February, and March. The zonal latitude bin from 20°S–30°S (not shown) has the same results as the 40°S–50°S latitude bin in that the DJF season and the December and January tropopause temperatures are decreasing over the 20-years with a Student's t-test significance of greater than 95%. However, the 30°S–40°S zonal latitude bin only shows that the DJF change is significant at greater than 95%. These colder tropopause temperatures over time might account for further "freeze-drying" of the moist tropospheric air that can move isentropically into the lower stratosphere at mid-latitudes further dehydrating the hygropause regions in the mid-latitude. The significant trend in the MERRA tropopause temperature from 1986–2005 mirrors the results found by Santer et al. (2003) and Seidel and Randel (2006) from the ECMWF and NCEP/NCAR reanalysis data sets and radiosonde observations respectively. Both studies documented a tropopause that is trending colder by 0.7 K decade^{-1} and 0.41 $\pm$0.09 K decade^{-1}, respectively, and increasing in altitude by 120 m to 190 m and 64 $\pm$21 m decade^{-1}, respectively, over the 20 years to 25 years from 1979–1999 and 1980–2004, respectively. The MERRA data set produces tropopause temperature trends that are closer to values derived by Seidel and Randel (2006) and Zhou et al. (2001) of $\sim$0.5 K decade^{-1}. Changes in the tropopause height were not derived from SAGE II water vapor data because the altitude resolution of the data set is greater than 0.5 km. The study of altitude changes in the tropopause using MERRA data will be considered in future research.

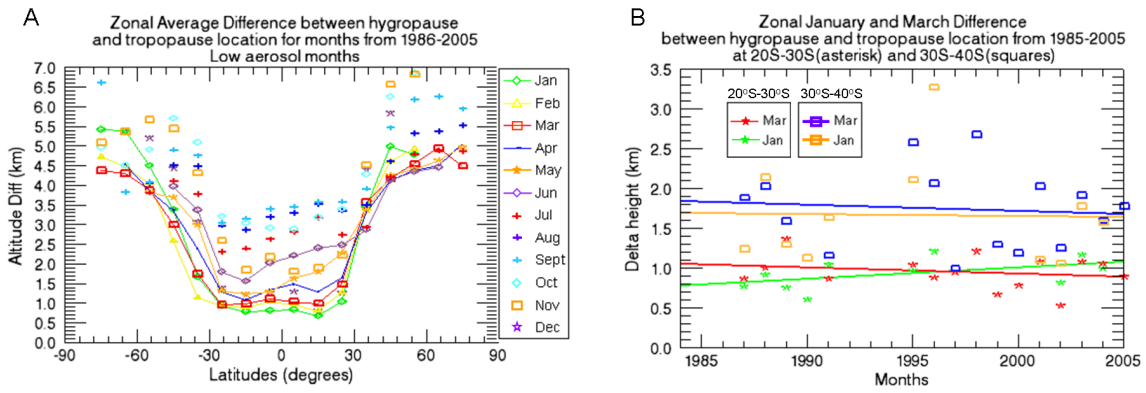

Figure 4.5: The left plot (A) is the January to December SAGE II 20-year average relative difference of the hygropause and tropopause heights for the low aerosol years. The right plot (B) shows January and March relative difference between the locations of the hygropause and tropopause where the January 20°S–30°S change over time (green) is significant at greater than 95%.

4.2 Tropical Broadening Analysis Using SAGE II Data

Tropical broadening has been discussed in terms of the expansion of the Hadley circulation and shifts of the subtropical and extra-tropical jets toward the poles (Davis and Rosenlof, 2012). A possible cause for the dehydration seen in the subtropical and mid-latitude lower stratosphere might be the broadening of the TTL into the extra-tropical latitudes. The colder temperatures associated with the tropical "cold trap" would have expanded into the mid-latitudes as part of the tropical broadening. Similarly, the higher latitudes would show more tropical characteristics, including increasingly tropical tropopause and hygropause altitudes. As a proxy for the process of tropical broadening, the height difference between the hygropause and tropopause was examined over the 20-year SAGE II water vapor record to determine if there is a significant change in the mid-latitude that mirrors the TTL characteristics possibly suggesting expansion of tropical characteristics into the mid-latitudes.

March is the seasonal month for the hygropause minimum, so the December through March monthly and the DJF seasonal transport barrier characteristics at

the tropics and sub-tropics were studied for long-term trends to account for the decrease seen in the March hygropause 20-year record. The hygropause and tropopause altitudes are determined from the SAGE II data where the tropopause height is provided with the SAGE II product as a meteorological parameter taken from the NCEP temperature and pressure heights ancillary data set. The 20-year average zonal monthly altitude difference between the hygropause and tropopause over 10-degree latitude bins are shown in Figure 4.5A along with the time series of the zonal mean height difference between the hygropause and tropopause in January and March for the sub-tropics and mid-latitude (Figure 4.5B). The relative difference in the location of the hygropause and tropopause is approximately 1 km in the tropics and expands to approximately 4 km to 6 km in the high latitudes as shown in Figure 4.5A. Only the month of January in the latitude bin from 20°S–30°S shows a significant trend of increasing differential height between the hygropause and tropopause (95% Student's *t*-test). Such a change is opposite from what we expect from the tropical broadening, but consistent with an increase of upwelling as a result of the Brewer-Dobson circulation. The observed variance is likely a response to an increase of the vertical distance between the tropopause and hygropause after 2000, which appears to be consistent with an increase of Brewer-Dobson circulation suggested by Randel et al. (2007).

4.3 Potential Vorticity and Jet Analysis

The transport barrier at the tropopause has been traditionally defined by a thermal gradient where the lowest temperature in this vertical thermal gradient or "cold trap" was the region in the tropopause layer where dehydration of tropospheric air occurred as it was being transported into the lower stratosphere (Brewer, 1949). Additional research has built on this seminal work highlighting that a horizontal thermal gradient might also be involved in the dehydration of the stratospheric air as moist tropospheric air traveled through the TTL region in the tropics and sub-tropics (Holton

and Gettelman, 2001). Horizontal thermal gradients provide additional dynamic responses at the tropopause that affect the transport of air parcels from the troposphere to the stratosphere, especially in the zonal mid- and high-latitudes where episodic dynamic events such as large cyclones and tropopause folds can significantly change the thermal profile of the tropopause layer (Stohl et al., 2003). It is because of these dynamic responses from both vertical and horizontal thermal gradients that the potential vorticity (PV) contours, which contain both absolute vorticity and potential temperature, were first used by Reed (1955) and later refined by Holton et al. (1995). The extra-tropical tropopause is located by definition at the PV contour around 2 PVU, where PVU is the standard PV unit of 10^{-6} $m^2s^{-1}K$ kg^{-1}.

Kunz et al. (2011) showed the sub-tropical jet and the thermal tropopause were approximately bounded by the ± 2 and ± 4 PVU contours—negative in the Southern Hemisphere (SH), positive in the Northern Hemisphere (NH). The sharpness of the PV gradients and the strength of the sub-tropical jet determine the extent for the transport of air across the quasi-isentropic barrier in the sub-tropical/extra-tropical regions. A larger PV gradient indicates a stronger jet and less isentropic transport across the dynamic barrier. To look for changes at the transport barrier in the sub-tropical and mid-latitude regions, the Southern Hemisphere—which shows more zonal uniformity in the PV contours compared to the Northern Hemisphere—PV and maximum sub-tropical jet Uwind speeds and location were analyzed.

The Southern Hemisphere has a more uniform zonal circulation in the extra-tropics as a result of a lack of topographical features that would introduce wave dynamics into the zonal atmospheric circulation. Because of this uniformity, the SH jet characteristics are examined using the NCEP and MERRA data. The NCEP meteorological data show that the strongest zonal winds associated with the SH sub-tropical jet are located at a pressure level of 200 mb at approximately 30°S, while the strongest zonal winds of the SH extra-tropical jet are at a pressure level of 250 mb at approximately

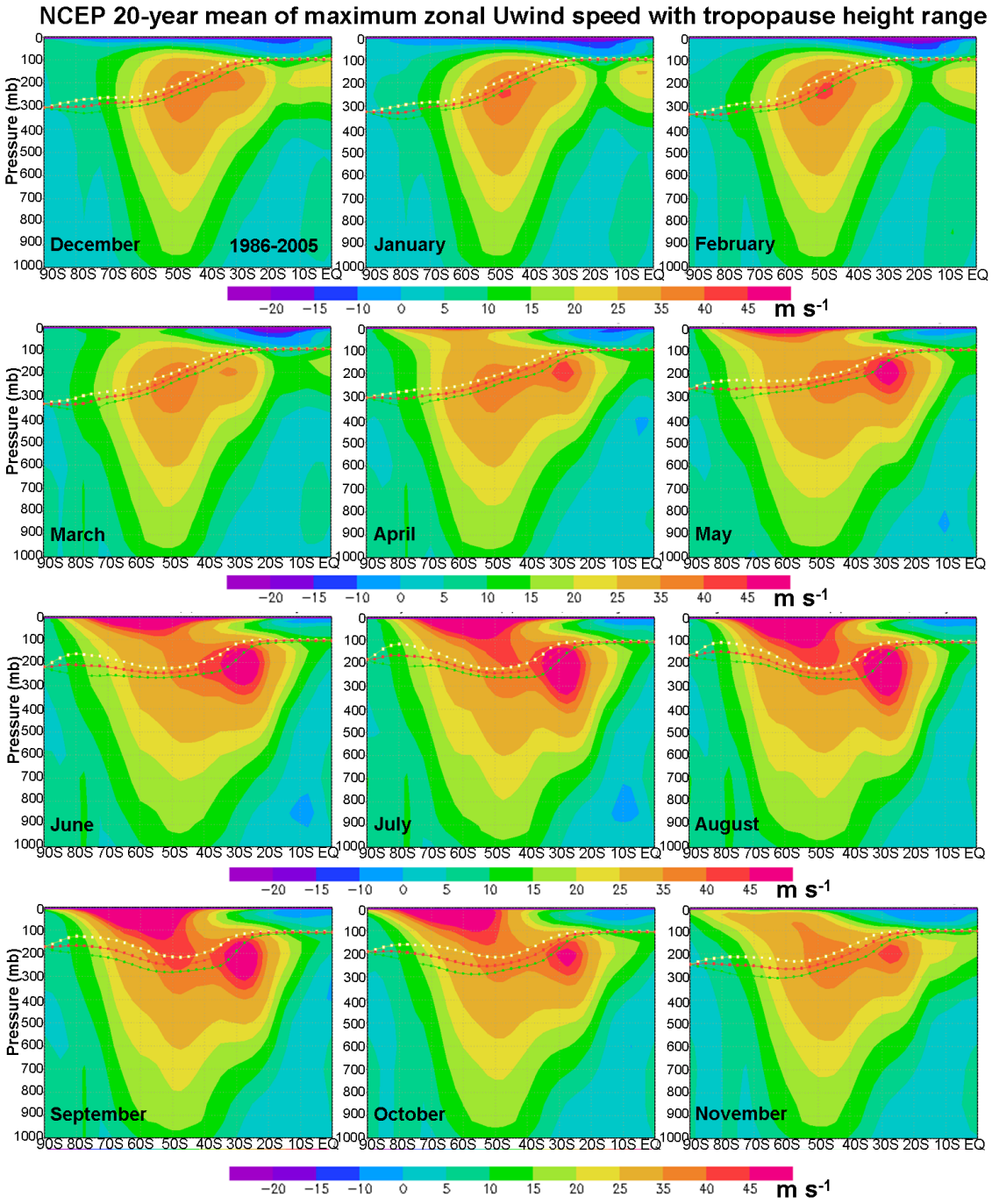

Figure 4.6: NCEP maximum southern Uwind composites for each month from 1986–2005 (December composites from 1985–2004) with zonal maximum (white), minimum (green), and mean tropopause (red) locations shown (dotted lines). The polar jet located above 100 mb has central latitude of ∼60°S and is present from April to November with the sub-tropical jet located at ∼30°S at the bottom of the TTL. December to March has a weak subtropical jet with the strongest winds located in the same region where the top of the extra-tropical jet is located (∼45°S).

45°S (Figure 4.6). For the DJF season, the extra-tropical jet dominates as the maximum zonal Uwind at the pressure level of 200 mb. Analysis of the maximum zonal Uwind speeds using the MERRA data does not show any statistically significant trend in the seasonal (DJF, MAM, JJA, SON) maximum Uwind speed for the period from 1986–2005. The analysis of the MERRA 200 mb data has jet features similar to the NCEP data with the JJA season having the fastest maximum zonal Uwind speeds (between 38 m s^{-1} and 44 m s^{-1}) and located between 27°S and 30°S and the DJF and MAM seasons having the weakest zonal Uwind speeds (between 26 m s^{-1} and 34 m s^{-1}) and located between 45°S and 50°S. The monthly 20-year trend in maximum zonal Uwind speed and location was not found to be statistically significant in the MERRA data implying that the transport barrier was not affected by a stronger jet in the extra-tropical tropopause layer. The PV contours that bound the jet were analyzed next to determine if the location of the jet during the months preceding the zonal monthly water vapor minimum have changed, possibly affecting transport across the tropopause in the extra-tropics.

Figure 4.7a shows the latitude location of the monthly averaged MERRA PV contours at −4 PVU and −2 PVU from 1986–2005. Only the December −2 PVU and the March −4 PVU 20-year trends test at greater than 95% significance using a Student's t-test. The December −4 PVU, however, is at the 94.98% level of significance. The significant December trends on the −4 PVU and −2 PVU levels show a steady movement towards the southern pole with a small but insignificant change in the PV location at the 200 mb height. The movement in the PV latitude location between the −2 PVU and −4 PVU PV contours (Figure 4.7, plot b) shows a statistically insignificant widening over the 20-year time period. This lack of significance in the zonal width of the PV bands that defines the zonal sub-tropical jet region does not indicate an overall change in the strength of the dynamic barrier for isentropic transport. Since the southern sub-tropical jet is most often bracketed between the

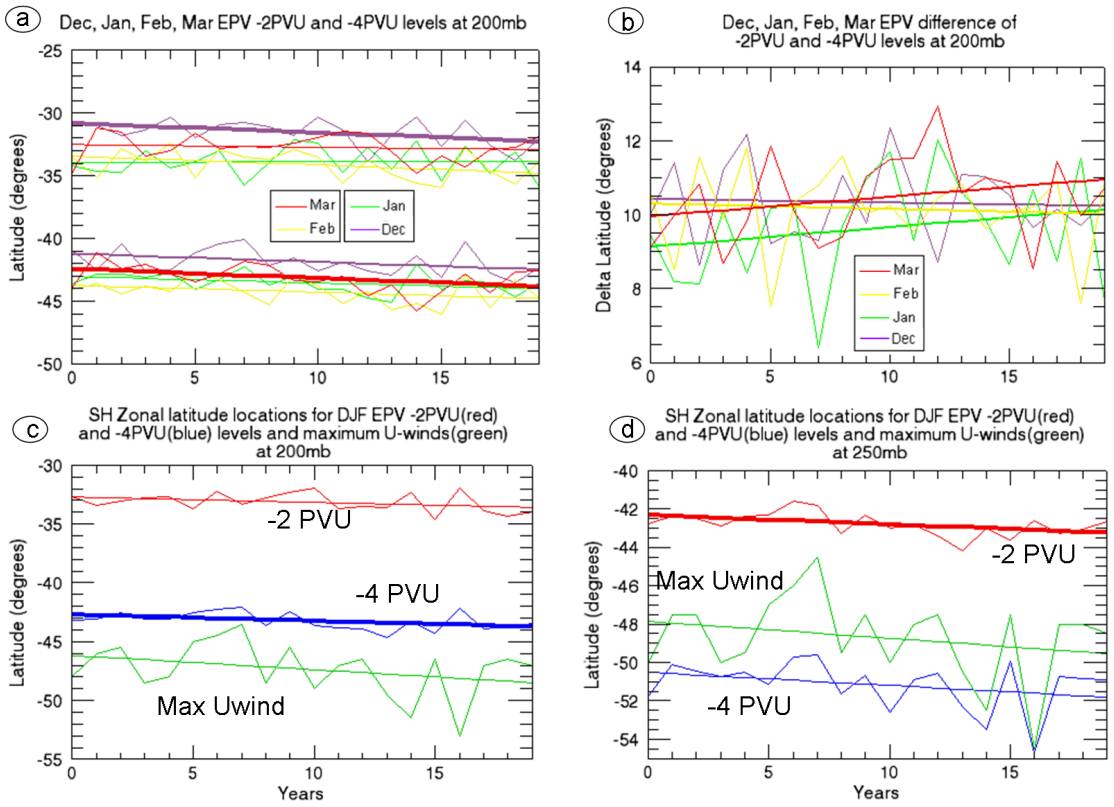

Figure 4.7: Plots a–b: Seasonal −4 PVU and −2 PVU PV locations at 200 mb and the latitude differences between the two PV contours. The DJF seasonal 20-year trends in the location of the PV −4 PVU (Blue) and the −2 PVU (Red) gradients. Bold trend lines denote greater than 95% significance levels. Plots c–d: Location of the maximum zonal Uwind (green) is within the seasonal zone of the PV jet-stream contours at 250 mb, but outside the seasonal PV contours at 200 mb.

−4 PVU and the −2 PVU contours (Kunz et al., 2011), the significant shifting of the December PV levels at 200 mb towards the poles indicates that the sub-tropical jet might also be shifting to the poles. A poleward shift in the sub-tropical jet has been documented by Bengtsson et al. (2006) using ERA-40 data showing that a jet shift towards the poles might be caused by enhanced sea-surface temperatures (SST). Hu and Fu (2007) have documented a poleward shift between 2°–4.5° in zonal latitude in the Hadley cell which is bounded on the poleward edge by the sub-tropical jet. Seidel et al. (2007) summarizes the current research into the widening of the tropical belt which is bounded by the sub-tropical jets in both hemispheres. This poleward

movement in the sub-tropical jets has been shown to affect the troposphere by moving the dry/rain zones on the surface, however there has been little discussion of how this movement in the jet and the Hadley cell edge would affect the transport barrier and lower stratospheric water vapor within the extra-tropical regions of the globe.

Extending the PV analysis to look for seasonal changes in the gradient and movement of the region bounded by the −2 PVU and −4 PVU PV contours that could affect the March hygropause, the DJF seasonal trends at two pressure levels were analyzed (Figure 4.7c–d). The trends of poleward shifts of the −4 PVU and −2 PVU contours at 200 mb in DJF are statistically significant at greater than 95% and 94.2% respectively. The MERRA Uwind data were used to determine the maximum Uwind location for the sub-tropical jet in the Southern Hemisphere. The maximum seasonal Uwind falls outside of the −4 PVU and −2 PVU brackets at 200 mb, but is bracketed by the PV lines at 250 mb, which is the level of maximum Uwind for most seasons. Variations in the maximum Uwind locations over the 20-year record are not statistically significant at either pressure level. The latitudinal differences between the −4 PVU and −2 PVU contours were statistically insignificant for all of the seasonal analyses performed, implying that the strength of the transport barrier was unchanged in both the magnitudes of the zonal PV gradients and the zonal maximum Uwind speeds over the 20-year time period. This analysis suggests that the SH subtropical jet as bounded by the −4 PVU and −2 PVU contours has shifted poleward in the austral summer season. This shift expands the TTL southward, allowing more dehydrated air to enter the tropical lower stratosphere in January. This change could also contribute to the enhanced hygropause in March.

4.4 Transport Barrier Analysis Summary and Conclusions

To help explain the water vapor variations seen over the 20-years of SAGE II water vapor data, the transport barrier between the troposphere and the stratosphere was

examined to determine if there were (1) temperature changes at the tropical tropopause that would account for the drier hygropause; (2) tropical broadening which would explain a more tropical-like dehydration of the subtropical/extra-tropical regions; and (3) changes in the subtropical/extra-tropical jet strength that would account for less transport isentropically across the transport barrier in the region of the subtropical ($\sim$30°) and extra-tropical ($\sim$45°) jets for the season preceding the March dehydrating hygropause.

A change in the strength of the sub-tropical jet would affect the transport barrier in the extra-tropics and could account for the water vapor variation in the 20-year March hygropause. The analysis of zonal PV contours and zonal maximum Uwinds did not show a statistically significant change in the strength of the sub-tropical jet. However, the PV contour lines at -2 PVU and -4 PVU, which have been shown to bound the sub-tropical jet in the sub-tropical region ($\sim$30°), did indicate a statistically significant movement of the SH sub-tropical jet towards the poles during the DJF and DJFM season over the 20-year time frame from 1986–2005. Such a poleward shift of the SH subtropical jets DJF could allow more dehydrated air entering the tropical stratosphere and therefore contribute to the strengthening and broadening of the hygropause in March.

The MERRA analysis shows a statistically significant decrease in the DJF tropical and sub-tropical tropopause temperature over the 20-year time period that can account for progressive dehydration at the tropical barrier. It is well known that the tropical "cold trap" mechanism freeze-dries the air moving across the tropical transport barrier (Fueglistaler et al., 2009) leading to a drier water vapor concentration above the tropopause. As this drier air is circulated upward and along isentropic temperature contours above the tropopause as seen in Figure 1.1(e) (i.e., rapid meridional transport above the tropopause), this drier air should be visible in the hygropause

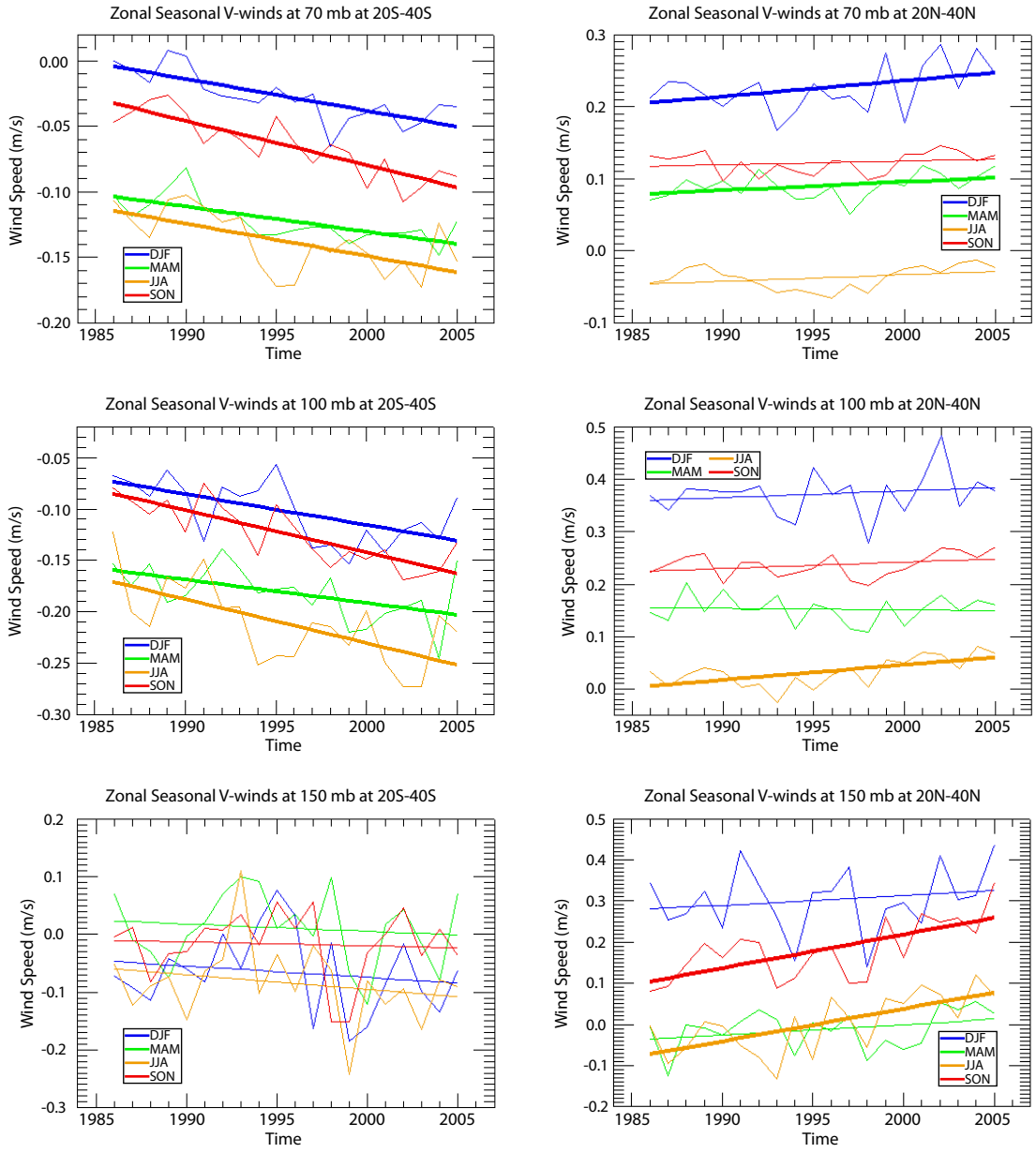

Figure 4.8: The zonal seasonal Vwind for the SH and NH at latitude bins between 20°–40°at pressure levels above the tropopause (70 mb, 100 mb, and 150 mb). Bold lines denote statistically significant trends in the zonal Vwind. Northward zonal Vwind direction is positive while a southward zonal Vwind direction is a negative.

and lower stratospheric water vapor retrievals from the tropics to the poles. Figure 4.8 shows the zonal Vwind speed for both the NH and the SH at the zonally averaged latitude bins from 20°–40° at three pressure levels above the tropopause. The SH zonal Vwind shows a statistically significant increase in the strength of the southward wind speed for all seasons at pressure levels above the tropopause (70 mb, 100 mb, and 150 mb) in the latitude region from 20°S–40°S indicating an enhanced lower branch of the Brewer-Dobson circulation that should influence the hygropause into the extra-tropical region.

CHAPTER V

DISCUSSION AND FUTURE WORK

Prior to the analysis performed in this thesis, the SAGE II water vapor product was recommended to be filtered for aerosol extinctions greater than 2×10^{-4} km^{-1} (Thomason et al., 2004) which eliminated all of the monthly mean water vapor data prior to 1996 near the tropopause (Chiou et al., 2006). Personal communications with L. W. Thomason (April 4, 2009) led to a filtering process that would retain the earlier part of the SAGE II water vapor data product at most altitudes and latitudes. Combining the filtered data into monthly means produced an enhancement to the SAGE II water vapor data set that extended the record from the late 1980s to the mid-2000s. This enhanced, filtered water vapor data set was then available for use to look at the long-term variations in zonal mean lower stratospheric water vapor and the hygropause over this 20-year timeframe.

Analysis of SAGE II water vapor data from 1986–2005 suggests a decadal drying and poleward spread of a drier hygropause that is consistent with results of HALOE, LIMS, and MLS data sets. These changes are greatest in March, when the hygropause is the driest. Analysis performed for this study shows a decrease of the tropical tropopause temperature during austral summer (DJF), an increase of the distance between the tropopause and hygropause in the SH subtropics in January, a poleward expansion of the Hadley circulation in the SH in December, and an increase of poleward meridional winds at 70 hPa during austral summer (DJF).

The lower stratospheric zonal water vapor trend seen in the long-term SAGE II water vapor retrievals from 1986–2005 is consistent with the trend seen in HALOE water vapor date from 1992–2005 (Randel et al., 2004). Chiou et al. (2006) also showed

good comparisons between the SAGE II and HALOE water vapor data, showing a decreasing trend in the lower stratosphere after 1996. These decreasing trends were at odds with the increasing lower stratospheric water vapor trends reported by Dvortsov and Solomon (2001), Rosenlof et al. (2001), and Oltmans et al. (2000) using balloon-bourn frost-point hygrometers at locations near Boulder, CO and Washington, DC in the Northern Hemisphere. The long-term negative variation seen in the SAGE II water vapor over the zonal mid-latitude Northern Hemisphere (Figure 3.5) is more consistent with the re-evaluated balloon-bourn frost-point data reported by Scherer et al. (2008) and Chiou et al. (2006), which shows no significant trend in water vapor from 1992–2005. This re-evaluation of the one data set that was showing an increasing trend in opposition to results from SAGE II and HALOE and concurrent research showing that the trend in the tropical tropopause temperatures is decreasing provides stronger evidence for a connection between decreasing tropopause temperatures and decreasing stratospheric water vapor (Randel et al., 2009).

The mechanisms reported in the literature that would account for such variations of the lower stratospheric water vapor and hygropause include cooling of the tropical tropopause temperature in the tropics (Zhou et al., 2001; Dvortsov and Solomon, 2001; Fueglistaler et al., 2005; Randel et al., 2006, 2009; Wright et al., 2011), a possible strengthening of upwelling and the Brewer-Dobson circulation (Randel et al., 2006; Garcia and Randel, 2008; Bonisch et al., 2010), and variations at the extra-tropical transport barrier that would affect the isentropic transport of air across the tropopause into the extra-tropical latitudes (Dessler et al., 1995; Hintsa et al., 1998; Ray et al., 2004). The results recorded in this thesis suggest that the decrease in the temperature of the "cold trap" and enhancement of the lower B-D circulation are the likely cause of the enhanced dehydration of the hygropause seen in the SAGE II water vapor. In addition, the poleward expansion of the SH portion of the Hadley circulation in December could also allow more dehydrated air entering the tropical

stratosphere, and contribute to the drying of the hygropause. Finally, the increasing strength of the lower branch of the B-D circulation, as shown by a strengthened poleward wind at 70 hPa would move this drier air into the extra-tropical latitudes leading to poleward spread of a drier hygropause.

Other studies have looked at the changes in the location and strength of the subtropical and extra-tropical jets and analysis showing the zonal tropical region is widening (i.e., tropical broadening) (Hu and Fu, 2007; Seidel and Randel, 2007; Hudson, 2011). These studies are components of the overall research on the variations in the zonal seasonal Hadley circulation. The question of whether changes in the Hadley cells can influence isentropic transport of moist tropospheric air into the extra-tropical lower stratosphere is still an area of active research. It has been shown that isentropic transport of tropospheric air masses in the extra-tropics does occur, however these are regional studies, which are not explicitly tied to the Hadley circulation (Poulida et al., 1996; Rood et al., 1997; Ray et al., 2004). Conclusions on whether the Hadley circulation is zonally changing over the 20-years from 1986–2005 rely on zonally averaged monthly means for this study. The Ertel's Potential Vorticity zonal seasonal contour analysis in the Southern Hemisphere does indicate that there is a poleward movement in the austral summer extra-tropical jet. It is left for future work to determine whether this variation in the proxy location for the zonal poleward edge of the Hadley cell influences the isentropic transport of tropospheric air into the extra-tropical lower stratosphere.

This work has raised some interesting and important questions, such as: What are the main processes for dehydration in the extra-tropical hygropause? Can the tropical broadening be linked to responses in trends in the Pacific Decadal Oscillation? How much of the variation in the hygropause and lower stratospheric water vapor can be attributed to a variation in the methane oxidation process? What is controlling the

seasonal height changes in the tropopause and hygropause, and is there a long-term variation present?

An open question remains as to the importance of the process of extra-tropical isentropic transport to the mid-latitude hygropause. Future work will require correlation between deep-convective over-shooting systems and the concurrent and lagging measurements of SAGE II water vapor in the same extra-tropical region. Since zonal mean data hide the phase change in the Pacific Decadal Oscillation, a finer temporal resolution and possibly a finer spatial resolution will be necessary to discern a link between variations in the hygropause and the Pacific Decadal Oscillation.

Future work will also include more extensive analysis of the tropopause altitude changes in the TTL and extra-tropical regions using the MERRA data set. Seidel and Randel (2007) have shown that the tropopause height has increased by hundreds of meters. The SAGE II data set has a resolution of greater than 500 meters, making it necessary to refine the SAGE II altitude resolution or use a different data set to look for relative changes between the hygropause and tropopause altitudes and the absolute trends, if any, in their location. A new version for the SAGE II data is planned to be released in 2012/2013 with an improved ancillary reference for the altitude of each event measurement. It is expected that this will allow better altitude resolution for the study of changes in the heights of both the water vapor minimum and the tropopause height, which will be imported from the MERRA data set.

Carrying forward with the success of the SAGE II mission, three SAGE III instruments were built. The SAGE III/Meteor-3M mission launched into orbit in December 2001 on a Russian satellite, operating and supplying science data until 2005. A second SAGE III mission will deliver another SAGE III instrument to the International Space Station in 2014. The SAGE series of products admit good vertical resolution and exhibit a natural consistency across missions because of a substantially proved and thoroughly validated occultation measurement technique. Future

research on the long-term variations in the hygropause and lower stratospheric water vapor will utilize these SAGE III water vapor retrievals to expand and enhance the analysis performed in this work. The aerosol filtering enhancement to the SAGE II water vapor product that distinguishes this research can be extended to the SAGE III water vapor retrievals, providing the opportunity to enhance SAGE data utility for trend studies.

REFERENCES

Archer, C. L. and Caldeira, K. (2008). Historical trends in the jet streams. *Geophys. Res. Lett.*, 35(L08803). doi:10.1029/2008GL033614.

Bengtsson, L., Hodges, K. I., and Roeckner, E. (2006). Storm Tracks and Climate Change. *J. of Climate*, 19:3518–3543. doi:10.1175/JCLI3815.1.

Bevington, P. R. and Robinson, D. K. (2003). *Data Reduction and Error Analysis for the Physical Sciences*. McGraw Hill, 3^{rd} edition. ISBN 0-07-247227-8.

Bonisch, H., Engel, A., Birner, T., Hoor, P., Tarasick, D. W., and Ray, E. A. (2010). On the structural changes in the Brewer-Dobson circulation after 2000. *Atmos. Chem. Phys. Discuss.*, 10:28399–28430. doi:10.5194/acpd-10-28399-2010.

Brewer, A. W. (1949). Evidence for a world circulation provided by the measurements of helium and water vapour distribution in the stratosphere. *Q. J. R. Meteorol. Soc.*, 75(326):351–363. doi:10.1002/qj.49707532603.

Chiou, E. W., McCormick, M. P., McMaster, L. R., Chu, W. P., Larsen, J. C., Rind, D., and Oltmans, S. (1993). Intercomparison of Stratospheric Water Vapor Observed by Satellite Experiments: Stratospheric Aerosol and Gas Experiment II Versus Limb Infrared Monitor of the Stratosphere and Atmospheric Trace Molecule Spectroscopy. *J. Geophys. Res.*, 98(D3):4875–4887. doi:10.1029/92JD01629.

Chiou, E. W., Thomason, L. W., and Chu, W. P. (2006). Variability of Stratospheric Water Vapor Inferred from SAGE II, HALOE, and Boulder (Colorado) Balloon Measurements. *J. of Climate*, 19:4121–4133. doi:10.1175/JCLI3841.1.

Cunnold, D. M., Chu, W. P., Barnes, R. A., McCormick, M. P., and Veiga, R. E. (1989). Validation of SAGE II Ozone Measurements. *J. Geophys. Res.*, 94(D6):8447–8460. doi:10.1029/JD094iD06p08447.

Davis, S. M. and Rosenlof, K. H. (2012). A Multidiagnostic Intercomparison of Tropical-Width Time Series Using Reanalyses and Satellite Observations. *J. of Climate*, 25:1061–1078. doi:10.1175/JCLI-D-11-00127.1.

Dessler, A. E., Hintsa, E. J., Weinstock, E. M., Anderson, J. G., and Chan, K. R. (1995). Mechanisms controlling water vapor in the lower stratosphere: "A tale of two stratospheres". *J. Geophys. Res.*, 100(D11):23167–23172. doi:10.1029/95JD02455.

Dessler, A. E. and Sherwood, S. C. (2004). Effect of convection on the summertime extratropical lower stratosphere. *J. Geophys. Res.*, 109(D23301). doi:10.1029/2004JD005209.

Dobson, G. M. B. (1956). Origin and distribution of the polyatomic molecules in the atmosphere. *Proceedings of the Royal Society of London. Series A, Mathematical and Physical Sciences*, 236(1205):187–193. doi:10.1098/rspa.1956.0127.

Dvortsov, V. L. and Solomon, S. (2001). Response of the stratospheric temperatures and ozone to past and future increases in stratospheric humidity. *J. Geophys. Res.*, 106(D7):7505–7514. doi:10.1029/2000JD900637.

Forster, P. M. d. F. and Shine, K. P. (1999). Stratospheric water vapour changes as a possible contributor to observed stratospheric cooling. *Geophys. Res. Lett.*, 26(21):3309–3312. doi:10.1029/1999GL010487.

Forster, P. M. d. F. and Shine, K. P. (2002). Assessing the climate impacts of trends in stratospheric water vapor. *Geophys. Res. Lett.*, 29(6):1086. doi:10.1029/2001GL013909.

Freie Universität Berlin (2012). Institute of Meteorology. *The Quasi-Biennial-Oscillation (QBO) Data Series*. Retrieved August 14, 2012, from http://www.geo.fu-berlin.de/en/met/ag/strat/produkte/qbo/index.html.

Fueglistaler, S., Bonazzola, M., Haynes, P. H., and Perter, T. (2005). Stratospheric water vapor predicted from the Lagrangian temperature history of air entering the stratosphere in the tropics. *J. Geophys. Res.*, 110(D08107). doi:10.1029/2004JD005516.

Fueglistaler, S., Dessler, A. E., Dunkerton, T. J., Folkins, I., Fu, Q., and Mote, P. W. (2009). Tropical Tropopause Layer. *Rev. Geophys.*, 47(RG1004). doi:10.1029/2008RG000267.

Garcia, R. R. and Randel, W. J. (2008). Acceleration of the Brewer-Dobson Circulation due to Increases in Greenhouse Gases. *J. Atmos. Sci.*, 65:2731–2739. doi:10.1175/2008JAS2712.1.

Gille, J. C. and Russell, III, J. M. (1984). The Limb Infrared Monitor of the Stratosphere: Experiment Description, Performance, and Results. *J. Geophys. Res.*, 89(D4):5125–5140. doi:10.1029/JD089iD04p05125.

Haynes, P. and Shuckburgh, E. (2000). Effective diffusivity as a diagnostic of atmospheric transport 1. Stratosphere. *J. Geophys. Res.*, 105(D18):22777–22794. doi:10.1029/2000JD900093.

Hintsa, E. J., Boering, K. A., Weinstock, E. M., Anderson, J. G., Gary, B. L., Pfister, L., Daube, B. C., Wofsy, S. C., Loewenstein, M., Podolske, J. R., Margitan, J. J., and Bui, T. P. (1998). Troposphere-to-stratosphere transport in the lowermost stratosphere from measurements of H_2O, CO_2, N_2O and O_3. *Geophys. Res. Lett.*, 25(14):2655–2658. doi:10.1029/98GL01797.

Holton, J. R. and Gettelman, A. (2001). Horizontal transport and the dehydration of the stratosphere. *Geophys. Res. Lett.*, 28(14):2799–2802. doi:10.1029/2001GL013148.

Holton, J. R., Haynes, P. H., McIntyre, M. E., Douglass, A. R., Rood, R. B., and Pfister, L. (1995). Stratosphere-troposphere exchange. *Rev. Geophys.*, 33(4):403–439. doi:10.1029/95RG02097.

Hoskins, B. J. (1991). Towards a PV-θ view of the general circulation. *Tellus A*, 43(4):27–35. doi:10.1034/j.1600-0870.1991.t01-3-00005.

Hu, Y. and Fu, Q. (2007). Observed poleward expansion of the Hadley circulation since 1979. *Atmos. Chem. Phys.*, 7:5229–5236. doi:10.5194/acp-7-5229-2007.

Hudson, R. D. (2011). Measurements of the movement of the jet streams at mid-latitudes, in the Northern and Southern Hemispheres, 1979 to 2010. *Atmos. Chem. Phys. Discuss.*, 11(11):31067–31090. doi:10.5194/acpd-11-31067-2011.

Kalnay, E., Kanamitsu, M., Kistler, R., Collins, W., Deaven, D., Gandin, L., Iredell, M., Saha, S., White, G., Woollen, J., Zhu, Y., Chelliah, M., Ebisuzaki, W., Higgins, W., Janowiak, J., Mo, K. C., Ropelewski, C., Wang, J., Leetmaa, A., Reynolds, R., Jenne, R., and Joseph, D. (1996). The NCEP/NCAR 40-year reanalysis project. *Bull. Am. Meteorol. Soc.*, 77(3):437–471. doi:10.1175/1520-0477(1996)077<0437:TNYRP>2.0.CO;2.

Kley, D., Stone, E. J., Henderson, W. R., Drummond, J. W., Harrop, W. J., Schmeltekopf, Thompson, T. L., and Winkler, R. H. (1979). *In Situ* Measurements of the Mixing Ratio of Water Vapor in the Stratosphere. *J. Atmos. Sci.*, 36(12):2513–2524. doi:10.1175/1520-0469(1979)036<2513:SMOTMR>2.0.CO;2.

Kunz, A., Konopka, P., Muller, R., and Pan, L. L. (2011). Dynamical tropopause based on isentropic potential vorticity gradients. *J. Geophys. Res.*, 116(D01110). doi:10.1029/2010JD014343.

Kutner, M. H., Nachtsheim, C. J., Neter, J., and Li, W. (2005). *Applied Linear Statistical Models*. McGraw-Hill/Irwin, New York, 5^{th} edition. ISBN 0-07-238688-6.

Lambert, A., Read, W. G., Livesey, N. J., Santee, M. L., Manney, G. L., Froidevaux, L., Wu, D. L., Schwartz, M. J., Pumphrey, H. C., Jimenez, C., Nedoluha, G. E., Cofield, R. E., Cuddy, D. T., Daffer, W. H., Drouin, B. J., Fuller, R. A., Jarnot, R. F., Knosp, B. W., Pickett, H. M., Perun, V. S., Snyder, W. V., Stek, P. C., Thurstans, R. P., Wagner, P. A., Waters, J. W., Jucks, K. W., Toon, G. C., Stachnik, R. A., Bernath, P. F., Boone, C. D., Walker, K. A., Urban, J., Murtagh, D., Elkins, J. W., and Atlas, E. (2007). Validation of the Aura Microwave Limb Sounder middle atmosphere water vapor and nitrous oxide measurements. *J. Geophys. Res.*, 112(D24S36). doi:10.1029/2007JD008724.

Liu, Y. S., Fueglistaler, S., and Haynes, P. H. (2010). Advection-condensation paradigm for stratospheric water vapor. *J. Geophys. Res.*, 115(D24307). doi:10.1029/2010JD014352.

Livesey, N. J. and Read, W. G. (2000). Direct retrieval of line-of-sight atmospheric structure from limb sounding observations. *Geophys. Res. Lett.*, 27(6):891–894. doi:10.1029/1999GL010964.

Livesey, N. J., Read, W. G., Filipiak, M. J., Froidevaux, L., Harwood, R. S., Jiang, J. H., Jimenez, C., Pickett, H. M., Pumphrey, H. C., Santee, M. L., Schwartz, M. J., Waters, J. W., and Wu, D. L. (2005). *EOS MLS Version 1.5 Level 2 data quality and description document*. Jet Propulsion Laboratory, California Institute of Technology, Pasadena, California, 91109-8099. Document D-32381, Version 1.51.

Livesey, N. J., Read, W. G., Lambert, A., Froidevaux, L., Harwood, R. S., Jiang, J. H., Jiang, Y. B., Kovalenko, L. J., Pickett, H. M., Pumphrey, H. C., Santee, M. L., Schwartz, M. J., Waters, J. W., and Wu, D. L. (2007). *EOS MLS Version 2.2 Level 2 data quality and description document*. Jet Propulsion Laboratory, California Institute of Technology, Pasadena, California, 91109-8099. Document D-32381, Version 2.2x-0.

McCormick, M. P. and Veiga, R. E. (1992). SAGE II Measurements of Early Pinatubo Aerosols. *J. Geophys. Res.*, 19(2):155–158. doi:10.1029/91GL02790.

Mote, P. W., Rosenlof, K. H., Holton, J. R., Harwood, R. S., and Waters, J. W. (1995). Seasonal variations of water vapor in the tropical lower stratosphere. *Geophys. Res. Lett.*, 22(9):1093–1096. doi:10.1029/95GL01234.

NASA Goddard Space Flight Center, GMAO (2012). NASA. *MERRA: MODERN ERA-RETROSPECTIVE ANALYSIS FOR RESEARCH AND APPLICATIONS*. Retrieved August 14, 2012, from http://gmao.gsfc.nasa.gov/research/merra/intro.php.

NASA Langley Research Center, Office of Public Affairs (1996). NASA. *SAGE II: Understanding the Earth's Stratosphere*. Retrieved August 14, 2012, from http://www.nasa.gov/centers/langley/news/factsheets/SAGE.html.

Nedoluha, G. E., Bevilacqua, R. M., and Hoppel, K. W. (2002). POAM III measurements of dehydration in the Antarctic and comparisons with the Arctic. *J. Geophys. Res.*, 107(D20). doi:10.1029/2001JD001184.

Oltmans, S. J. and Hofmann, D. J. (1995). Increase in lower-stratospheric water vapour at a mid-latitude Northern Hemisphere site from 1981 to 1994. *Nature*, 374:146–149. doi:10.1038/374146a0.

Oltmans, S. J., Vömel, H., Hofmann, D. J., Rosenlof, K. H., and Kley, D. (2000). The increase in stratospheric water vapor from balloonborne, frostpoint hygrometer measurements at Washington, D.C., and Boulder, Colorado. *Geophys. Res. Lett.*, 27(21):3453–3456. doi:10.1029/2000GL012133.

Poulida, O., Dickerson, R. R., and Heymsfield, A. (1996). Stratosphere-troposphere exchange in a midlatitude mesoscale convective complex 1. Observations. *J. Geophys. Res.*, 101(D3):6823–6836. doi:10.1029/95JD03523.

Press, W. H., Teukolsky, S. A., Vetterling, W. T., and Flannery, B. P. (1993). *Numerical Recipes in C – The Art of Scientific Computing*. Cambridge University Press, 2^{nd} edition. ISBN 0-521-43108-5.

Randel, W. J., Park, M., Wu, F., and Livesey, N. (2007). A Large Annual Cycle in Ozone above the Tropical Tropopause Linked to the Brewer-Dobson Circulation. *J. Atmos. Sci.*, 64:4479–4488. doi:10.1175/2007JAS2409.1.

Randel, W. J., Shine, K. P., Austin, J., Barnett, J., Claud, C., Gillett, N. P., Keckhut, P., Langematz, U., Lin, R., Long, C., Mears, C., Miller, A., Nash, J., Seidel, D. J., Thompson, D. W. J., Wu, F., and Yoden, S. (2009). An update of observed stratospheric temperature trends. *J. Geophys. Res.*, 114(D02107). doi:10.1029/2008JD010421.

Randel, W. J., Wu, F., Oltmans, S. J., Rosenlof, K., and Nedoluha, G. E. (2004). Interannual Changes of the Stratospheric Water Vapor and Correlations with Tropical Tropopause Temperatures. *J. Atmos. Sci.*, 61:2133–2148. doi:10.1175/1520-0469(2004)061<2133:ICOSWV>2.0.CO;2.

Randel, W. J., Wu, F., Vömel, H., Nedoluha, G. E., and Forster, P. (2006). Decreases in stratospheric water vapor after 2001: Links to changes in the tropical tropopause and the Brewer-Dobson circulation. *J. Geophys. Res.*, 111(D12312). doi:10.1029/2005JD006744.

Ray, E. A., Moore, F. L., Rosenlof, K. H., Davis, S. M., Boenisch, H., Morgenstern, O., Smale, D., Rozanov, E., Hegglin, M., Pitari, G., Mancini, E., Braesicke, P., Butchart, N., Hardiman, S., Li, F., Shibata, K., and Plummer, D. A. (2010). Evidence for changes in the stratospheric transport and mixing over the past three decades based on multiple data sets and tropical leaky pipe analysis. *J. Geophys. Res.*, 115(D21304). doi:10.1029/2010JD014206.

Ray, E. A., Rosenlof, K. H., Richard, E. C., Hudson, P. K., Cziczo, D. J., Loewenstein, M., Jost, H.-J., Lopez, J., Ridley, B., Weinheimer, A., Montzka, D., Knapp, D., Wofsy, S. C., Daube, B. C., Gerbig, C., Xueref, I., and Herman, R. L. (2004). Evidence of the effect of summertime midlatitude convection on the subtropical lower stratosphere from CRYSTAL-FACE tracer measurements. *J. Geophys. Res.*, 109(D18304). doi:10.1029/2004JD004655.

Read, W. G., Lambert, A., Bacmeister, J., Cofield, R. E., Christensen, L. E., Cuddy, D. T., Daffer, W. H., Drouin, B. J., Fetzer, E., Froidevaux, L., Fuller, R., Herman, R., Jamot, R. F., Jiang, J. H., Jiang, Y. B., Kelly, K., Knosp, B. W., Kovalenko, L. J., Livesey, N. J., Lui, H., Manney, G. L., Pickett, H. M., Pumphrey, H. C., Rosenlof, K. H., Sabounchi, X., Santee, M. L., Schwartz, M. J., Snyder, W. V.,

Stek, P. C., Su, H., Takacs, L. L., Thurstans, R. P., Vömel, H., Wagner, P. A., Waters, J. W., Webster, C. R., Weinstock, E. M., and Wu, D. L. (2007). Aura Microwave Limb Sounder upper tropospheric and lower stratospheric H_2O and relative humidity with respect to ice validation. *J. Geophys. Res.*, 112(D24S35). doi:10.1029/2007JD008752.

Read, W. G., Schwartz, M. J., Lambert, A., Su, H., Livesey, N. J., Daffer, W. H., and Boone, C. D. (2008). The roles of convection, extra-tropical mixing, and *in-situ* freeze-drying in the Tropical Tropopause Layer. *Atmos. Chem. Phys.*, 8:6051–6067. doi:10.5194/acp-8-6051-2008.

Read, W. G., Wu, D. L., Waters, J. W., and Pumphrey, H. C. (2004). Dehydration in the tropical tropopause layer: Implications from the UARS Microwave Limb Sounder. *J. Geophys. Res.*, 109(D06110). doi:10.1029/2003JD004056.

Reed, R. J. (1955). A study of a characteristic type of upper-level frontogenesis. *J. Meteorol.*, 12:226–237.

Remsberg, E. E., Natarajan, M., Lingenfelser, G. S., Thompson, R. E., Marshall, B. T., and Gordley, L. L. (2009). On the quality of the Nimbus 7 LIMS Version 6 water vapor profiles and distributions. *Atmos. Chem. Phys. Discuss.*, 9:17903–17935.

Remsberg, E. E., Russell, III, J. M., Gordley, L. L., Gille, J. C., and Bailey, P. L. (1984). Implications of the Stratospheric Water Vapor Distribution as Determined from the Nimbus 7 LIMS Experiment. *J. Atmos. Sci.*, 41(19):2934–2945.

Rienecker, M. M., Suarez, M. J., Gelaro, R., Todling, R., Bacmeister, J., Liu, E., Bosilovich, M. G., Schubert, S. D., Takacs, L., Kim, G.-K., Bloom, S., Chen, J., Collins, D., Conaty, A., da Silva, A., Gu, W., Joiner, J., Koster, R. D., Lucchesi, R., Molod, A., Owens, T., Pawson, S., Pegion, P., Redder, C. R., Reichle, R., Robertson, F. R., Ruddick, A. G., Sienkiewicz, M., and Woollen, J. (2011). MERRA - NASA's Modern-Era Retrospective Analysis for Research and Applications. *J. of Climate*, 24:3624–3648. doi:10.1175/JCLI-D-11-00015.1.

Rood, R. B., Douglass, A. R., Cerniglia, M. C., and Read, W. G. (1997). Synoptic-scale mass exchange from the troposphere to the stratosphere. *J. Geophys. Res.*, 102(D19):23467–23485. doi:10.1029/97JD01598.

Rosenlof, K. H., Oltmans, S. J., Kley, D., Russell, III, J. M., Chiou, E., Chu, W. P., Johnson, D. G., Kelly, K. K., Michelsen, H. A., Nedoluha, G. E., Remsberg, E. E., Toon, G. C., and McCormick, M. P. (2001). Stratospheric water vapor increases over the past half-century. *Geophys. Res. Lett.*, 28(7):1195–1198. doi:10.1029/2000GL012502.

Rosenlof, K. H. and Reid, G. C. (2008). Trends in the temperature and water vapor content of the tropical lower stratosphere: Sea surface connection. *J. Geophys. Res.*, 113(D06107). doi:10.1029/2007JD009109.

Russell, III, J. M., Gille, J. C., Remsberg, E. E., Gordley, L. L., Bailey, P. L., Fischer, H., Girard, A., Drayson, S. R., Evans, W. F. J., and Harries, J. E. (1984). Validation of Water Vapor Results Measured by the Limb Infrared Monitor of the Stratosphere Experiment on NIMBUS 7. *J. Geophys. Res.*, 89(D4):5115–5124. doi:10.1029/JD089iD04p05115.

Russell, III, J. M., Gordley, L. L., Park, J. H., Drayson, S. R., Hesketh, W. D., Cicerone, R. J., Tuck, A. F., Frederick, J. E., Harries, J. E., and Crutzen, P. J. (1993). The Halogen Occultation Experiment. *J. Geophys. Res.*, 98(D6):10777–10797. doi:10.1029/93JD00799.

Santer, B. D., Wehner, M. F., Wigley, T. M. L., Sausen, R., Meehl, G. A., Taylor, K. E., Ammann, C., Arblaster, J., Washington, W. M., Boyle, J. S., and Brüggemann, W. (2003). Contributions of Anthropogenic and Natural Forcing to Recent Tropopause Height Changes. *Science*, 301(5632):479–483. doi:10.1126/science.1084123.

Scherer, M., Vömel, H., Fueglistaler, S., Oltmans, S. J., and Staehelin, J. (2008). Trends and variability of midlatitude stratospheric water vapour deduced from the re-evaluated Boulder balloon series and HALOE. *Atmos. Chem. Phys.*, 8:1391–1402. doi:10.5194/acp-8-1391-2008.

Schoeberl, M. R. (2004). Extratropical stratosphere-troposphere mass exchange. *J. Geophys. Res.*, 109(D13303). doi:10.1029/2004JD004525.

Schoeberl, M. R., Douglass, A. R., Hilsenrath, E., Bhartia, P. K., Beer, R., Waters, J. W., Gunson, M. R., Froidevaux, L., Gille, J., Barnett, J. J., Levelt, P., and DeCola, P. (2006). Overview of the EOS Aura Mission. *IEEE Transactions on Geoscience and Remote Sensing*, 44(5):1066–1074. doi:10.1109/TGRS.2005.861950.

Seidel, D. J., Fu, Q., Randel, W. J., and Reichler, T. J. (2007). Widening of the tropical belt in a changing climate. *Nature*, 374:1–4. Progress Article. doi:10.1038/374146a0.

Seidel, D. J. and Randel, W. J. (2006). Variability and trends in the global tropopause estimated from radiosonde data. *J. Geophys. Res.*, 111(D21101). doi:10.1029/2006JD007363.

Seidel, D. J. and Randel, W. J. (2007). Recent widening of the tropical belt: Evidence from tropopause observations. *J. Geophys. Res.*, 112(D20113). doi:10.1029/2007JD008861.

Sokolik, I. (2008). Global radiation balance. In Jorgensen, E., editor, *Encyclopedia of Ecology*, pages 214–218. Elsevier. ISBN 0444520333.

Solomon, S., Qin, D., Manning, M., Alley, R. B., Berntsen, T., Bindoff, N. L., Chen, Z., Chidthaisong, A., Gregory, J. M., Hegerl, G. C., Heimann, M., Hewitson, B., Hoskins, B. J., Joos, F., Jouzel, J., Kattsov, V., Lohmann, U., Matsuno, T., Molina,

M., Nicholls, N., Overpeck, J., Raga, G., Ramaswamy, V., Ren, J., Rusticucci, M., Somerville, R., Stocker, T. F., Whetton, P., Wood, R. A., and Wratt, D. (2007). Contribution of Working Group I to the Fourth Assessment Report of the Intergovernmental Panel on Climate Change. In Solomon, S., Qin, D., Manning, M., Chen, Z., Marquis, M., Averyt, K. B., Tignor, M., and Miller, H. L., editors, *Climate Change 2007: The Physical Science Basis*. Cambridge University Press, Cambridge, United Kingdom and New York, NY, USA.

Solomon, S., Rosenlof, K., Portmann, R., Daniel, J., Davis, S., Sanford, T., and Plattner, G. (2010). Contributions of stratospheric water vapor to decadal changes in the rate of global warming. *Science*, 327(5970):1219–1223. doi:10.1126/science.1182488.

Stohl, A., Wernli, H., James, P., Bourqui, M., Forster, C., Liniger, M. A., Seibert, P., and Sprenger, M. (2003). A new perspective on stratosphere-troposphere exchange. *Bull. Am. Meteorol. Soc.*, 84:1565–1573. doi:10.1175/BAMS-84-11-1565.

Taha, G., Thomason, L. W., and Burton, S. P. (2004). Comparison of the Stratospheric Aerosol and Gas Experiment (SAGE) II version 6.2 water vapor with balloon-borne and space-based instruments. *J. Geophys. Res.*, 109(D18313). doi:10.1029/2004JD004859.

Tandon, N. F., Polvani, L. M., and Davis, S. M. (2011). The response of the tropospheric circulation to water vapor-like forcings in the stratosphere. *J. of Climate*, 24:5713–5720. doi:10.1175/JCLI-D-11-00069.1.

Thomason, L. W., Burton, S., Iyer, N., Zawodny, J., and Anderson, J. (2004). A revised water vapor product for the Stratospheric Aerosol and Gas Experiment (SAGE) II version 6.2 data set. *J. Geophys. Res.*, 109(D06312). doi:10.1029/2003JD004465.

Thompson, D. W. J. and Solomon, S. (2009). Understanding recent stratospheric climate change. *J. of Climate*, 22:1934–1943. doi:10.1175/2008JCLI2482.1.

Vömel, H., Oltmans, S. J., Hofmann, D. J., Deshler, T., and Rosen, J. M. (1995). The evolution of the dehydration in the Antarctic stratospheric vortex. *J. Geophys. Res.*, 100(D7):13919–13926. doi:10.1029/95JD01000.

Wang, P. K. (2003). Moisture plumes above thunderstorm anvils and their contributions to cross-tropopause transport of water vapor in midlatitudes. *J. Geophys. Res.*, 108(D6):4194. doi:10.1029/2002JD002581.

Waters, J. W., Froidevaux, L., Harwood, R. S., Jarnot, R. F., Pickett, H. M., Read, W. G., Siegel, P. H., Cofield, R. E., Filipiak, M. J., Flower, D. A., Holden, J. R., Lau, G. K., Livesey, N. J., Manney, G. L., Pumphrey, H. C., Santee, M. L., Wu, D. L., Cuddy, D. T., Lay, R. R., Loo, M. S., Perun, V. S., Schwartz, M. J., Stek, P. C., Thurstans, R. P., Boyles, M. A., Chandra, K. M., Chavez, M. C., Chen, G.-S., Chudasama, B. V., Dodge, R., Fuller, R. A., Girard, M. A., Jiang, J. H., Jiang,

Y., Knosp, B. W., LaBelle, R. C., Lam, J. C., Lee, K. A., Miller, D., Oswald, J. E., Patel, N. C., Pukala, D. M., Quintero, O., Scaff, D. M., Snyder, W. V., Tope, M. C., Wagner, P. A., and Walch, M. J. (2005). The Earth Observing System Microwave Limb Sounder (EOS MLS) on the Aura Satellite. *IEEE Transactions on Geoscience and Remote Sensing*, 44(5):1075–1092. doi:10.1109/TGRS.2006.873771.

Webster, P. J. (2004). 1. The Elementary Hadley Circulation. In Diaz, H. and Bradley, R., editors, *The Hadley Circulation: Present, Past and Future (Advances in Global Change Research)*, volume 21, pages 9–60. Cambridge University Press. ISBN 1-4020-2943-8.

Wright, J. S., Fu, R., Fueglistaler, S., Lui, Y. S., and Zhang, Y. (2011). The influence of summertime convection over Southeast Asia on water vapor in the tropical stratosphere. *J. Geophys. Res.*, 116(D12302). doi:10.1029/2010JD015416.

Yue, G. K., McCormick, M. P., Chu, W. P., Wang, P., and Osborn, M. T. (1989). Comparative studies of aerosol extinction measurements made by the SAM II and SAGE II satellite experiments. *J. Geophys. Res.*, 94(D6):8412–8424. doi:10.1029/JD094iD06p08412.

Zhou, X. L., Geller, M. A., and Zhang, M. (2001). Cooling trend of the tropical cold point tropopause temperatures and its implications. *J. Geophys. Res.*, 106(D2):1511–1522. doi:10.1029/2000JD900472.